Simulation of organic aerosol, its precursors and related oxidants in the Landes pine forest in south-western France: Need to account for domain specific land-use and physical conditions

Arineh Cholakian[1,2,4], Matthias Beekmann[2], Guillaume Siour[3], Isabelle Coll[3], Manuela Cirtog[3], Elena Ormeño[5], Pierre-Marie Flaud[1], Emilie Perraudin[1], and Eric Villenave[1]

[1]Univ. Bordeaux, CNRS, EPOC, EPHE, UMR 5805, F-33405 Talence Cedex, France
[2]Université de Paris Cité and Univ Paris Est Créteil, CNRS, LISA, F-75013, Paris, France
[3]Univ Paris Est Créteil and Université de Paris Cité, CNRS, LISA, F-94010, Créteil, France
[4]LMD UMR CNRS 8539, ENS, Ecole Polytechnique, Institut Pierre Simon Laplace (IPSL), Palaiseau, France.
[5]CNRS, Aix Marseille Univ, IRD, Avignon Univ, IMBE, 13397 Marseille, France.

Correspondence: Arineh Cholakian (arineh.cholakian@lmd.ipsl.fr)

Abstract. Organic aerosol (OA) still remains one of the most difficult components of the atmospheric aerosols to simulate, given the multitude of its precursors, the uncertainty of its formation pathways and the lack of measurements of its detailed composition. The LANDEX project (The LANDes Experiment), during its intensive field campaign in summer 2017, gives us not only the opportunity to compare biogenic secondary OA ($BSOA$), but also its precursors and oxidants obtained within and above the Landes forest canopy, to simulations performed with CHIMERE, a state-of-the-art regional Chemistry-Transport Model. The Landes forest is situated in the south-western part of France, and is one of the largest anthropized forests in Europe (1 million ha), composed by a majority of maritime pine trees, strong terpenoid emitters, providing a large potential for biogenic SOA formation. In order to simulate OA build-up in this area, a specific model configuration set-up, adapted to the local peculiarities was necessary. As the forest is non-homogeneous, with interstitial agricultural fields, high-resolution 1 km simulations over the forest area were performed. $BVOC$ emissions were predicted by MEGAN, but specific landcover information needed to be used, chosen from the comparison of several high-resolution landcover databases. Moreover, the tree species distribution needed to be updated for the specific conditions of the Landes forest. In order to understand the canopy effect in the forest, canopy effects on vertical diffusivity, winds and radiation were implemented in the model in a simplified way. The refined simulations show a redistribution of $BVOC$s with a decrease in isoprene and an increase in terpenoid emissions with respect to the standard case, in line with observations. Corresponding changes on simulated $BSOA$ sources are tracked. Very low night-time ozone, sometimes near zero, remains overestimated in all simulations. This has implications to the night-time oxidant budget, including NO_3. Despite careful treatment of physical conditions, simulated $BSOA$ is overestimated in the most refined simulation. Simulations are also compared to air quality sites surrounding the Landes forest, reporting a more realistic simulation in these stations in the most refined test case. Finally, the importance of the sea breeze system which also impacts species concentrations inside the forest is made evident.

1 Introduction

Forested areas - either natural or artificially managed - induce different biosphere-atmosphere interactions, leading to complex physico-chemical processes that have a significant impact on the composition of the atmosphere on regional and global scales. They are responsible for 90% of volatile organic compound (VOC) emissions worldwide (Delmas et al., 2005), mainly isoprene, but also monoterpenes, and other VOCs (Guenther et al., 2012). The initial oxidation steps of these compounds happens by reacting with OH and NO_3 radicals, and ozone (O_3) (Seinfeld and Pandis, 2016). When undergoing rapid oxidation processes, biogenic VOCs ($BVOC$s) generate various oxidation products, which may affect the atmospheric oxidative budget (Hallquist et al., 2009). Part of these products have sufficiently low vapor pressures or large enough Henry's law constants to further form biogenic secondary organic aerosols ($BSOA$s). $BVOC$ oxidation processes are strongly affected by anthropogenic emissions, especially NO_x availability (e.g. Sartelet et al. (2012); Shrivastava et al. (2019)), and depending to this availability, the associated oxidation pathways may lead to O_3 formation. The complexity of this system and the eventual impact of their oxidation products on air quality and human health make forested areas a good environment to isolate and focus on only specific parts of the underlying chemical mechanisms.

While this system has been investigated in many studies for different types of forests (e.g. Hellén et al. (2018) for boreal forests; Shrivastava et al. (2019) for tropical forests), uncertainties still subsist in the quantification of the mixture of emitted $BVOC$ species, the formation mechanisms and yields of secondary products (Hallquist et al., 2009), the interactions between biogenic and anthropogenic emissions (e.g. Xu et al. (2015)), as well as the impact of produced aerosols on regional climate (Gray Bé et al. (2017), via cloud activation of $BSOA$ species) or on global climate (Kulmala et al. (2004); Sporre et al. (2019)).

Hantson et al. (2017) estimate that, for a 30-year period from 1971-2000, the global emissions of isoprene and monoterpenes are around 300 TgC.yr^{-1} and 26 TgC.yr^{-1} respectively. While this means that globally isoprene is the major precursor for the formation of $BSOA$s due to the sheer amount of its emission, monoterpenes have to be considered as well due to higher $BSOA$ formation yields, varying from 10 to 60% (Griffin et al. (1999); Lee et al. (2006a); Lee et al. (2006b); Ng et al. (2007)). For example, for the SOAS study in summer 2013 in Southeastern US, Xu et al. (2015) found a more than 50% contribution of the monoterpene + NO_3 reaction pathway to night-time $BSOA$ formation. As NO_3 is generated from the NO_2 + O_3 reaction, this latter pathway provides one of the possible links between anthropogenic and biogenic emissions. Of course, this distinction between precursors becomes more apparent locally, depending on the ecosystem characteristics in each region (types of trees, climate, etc.), and is also mediated by the oxidant availability.

This study aims to put into perspective that, while we possess all the information needed to simulate the global state of $BVOC$s and their oxidation products, locally this is not the case. At the local level, numerical models require the use of detailed information of landcover, emission rates, chemical gas phase, aerosols schemes and aerosol – climate interaction mechanisms. We will be focusing on one specific ecosystem, in an effort to pinpoint the local characteristics of the Landes forest and their effect on the local air quality and atmospheric chemistry.

The Landes forest is one of the largest European forests, covering an area of about 1 million hectares in southwestern France. Its dominant tree species is maritime pine, Pinus pinaster Aiton., which is known to be a strong α and β-pinene emitter (Simon et al., 2001). Due to its rather homogeneous character, the Landes forest is an interesting region to study and to model $BVOC$-Oxidants-SOA-climate interactions. The LANDEX project (LANDEX, Landes Experiment: Formation and fate of secondary organic aerosols generated in the Landes forest) aimed at characterizing secondary organic aerosol formation observed in this monoterpene-rich environment. In the frame of LANDEX, a field campaign bringing together a dozen French and international partners was held in June and July 2017 at an instrumented site (Salles-Bilos) within the forest. Special care was taken to extensive characterization of $BVOC$ species (Mermet et al., 2019), to measurements of radical species and of OH reactivity (Bsaibes et al., 2020). Mermet et al. (2021) analyzed $BVOC$ and radical/oxidant species' abundance at Salles-Bilos and concluded that the reaction of β-caryophyllene (a sesqui-terpene) with O_3 contributes most strongly to $BVOC$ reactivity within the forest canopy. Frequent episodes of night-time new particle formation (NPF) have been observed during this campaign as well as prior campaigns which has been linked to $BVOC$ oxidation processes (Kammer et al. (2018); Kammer et al. (2020)). During the summer 2018 follow-up Cervoland experiment (a spin-off of LANDEX), Li et al. (2020) made evident the presence of very low volatile suitable precursors (diterpene species) by high resolution mass spectrometry analyses. Campaign results are still under active investigation. The LUCAS project (Land use, regional climate and atmospheric chemistry: the impact of forested surfaces on cloud enhancement and air quality in south-west France) within the LABEX COTE (LabEx (2023)) extends LANDEX objectives by aiming at investigating the impact of $BSOA$ from the Landes forest on regional climate and precipitation through formation of cloud condensation nuclei. A second goal is to study the impact of future climate change and forest management practices on the regional $BVOC$-SOA system.

A prerequisite for addressing objectives of the LUCAS project is to set-up a suitable modelling framework for addressing $BVOC$ emissions and subsequent SOA formation specifically tailored for the Landes forest. Our paper aims at constructing such a framework, by using the well referenced French and European CHIMERE model (Menut et al. (2013); CHIMERE (2023)), and to subsequently add detailed information for the Landes area. This includes specific information on landcover, on tree species distribution, on $BVOC$ emission factors, on detailed anthropogenic emissions, and on a specific dynamical treatment of the forest canopy. The paper carefully records the impact of these updates on atmospheric composition, $BSOA$ formation pathways and how they influence the agreement with observations from the LANDEX 2017 campaign. A second goal of this work is to use the CHIMERE model to provide 2D concentration fields at the surface, on the one hand to interpret the spatial representativeness of the Salles-Bilos measurement site, and on the other hand to provide insight into the link between transport and chemical processes.

The paper is organized as follows: after this introductive section, section 2 provides information on the campaign measurements and air quality network observations used in the study. Section 3 describes successive inclusion of information specific to the Landes forest in the standard version of CHIMERE. Section 4 evaluates the induced changes in the time series of the different species and explores $BSOA$ formation pathways. Section 5 presents a case study showing that both chemistry and transport processes affect species concentration at the measurement site. In the end, conclusions and perspectives are presented.

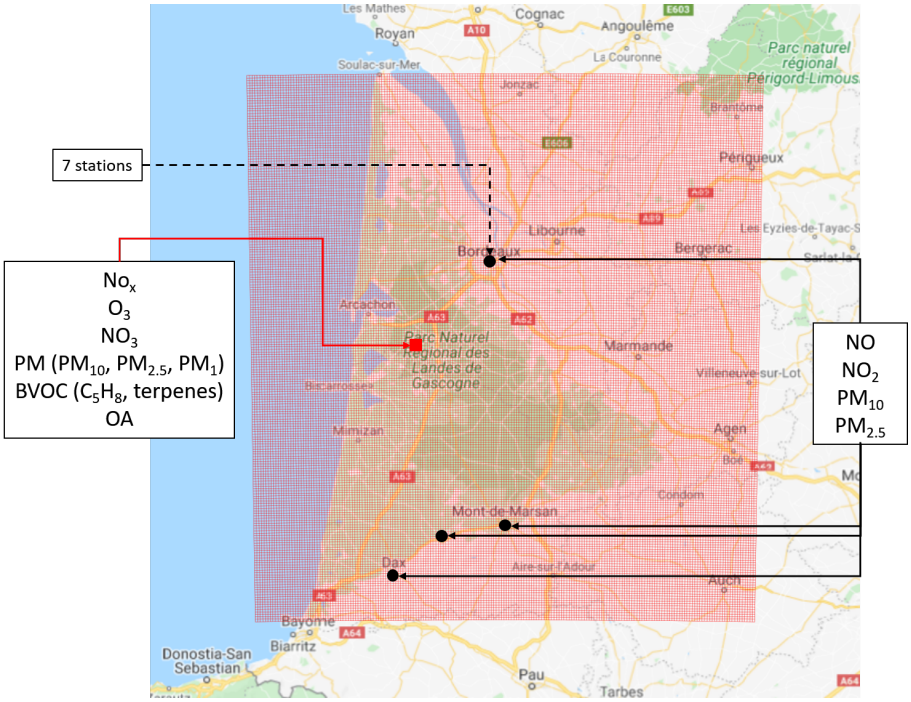

Figure 1. Measurements and monitoring stations in the Landes region and the high resolution simulation domain (horizontal resolution of 1 km). Black dots represent where the used air quality stations are located, the red circle shows the main measurement site in Salles-Bilos. Note that the northern point located on the city of Bordeaux regroups 7 stations (not shown separately because of their proximity). © OpenStreetMap contributors 2022. Distributed under the Open Data Commons Open Database License (ODbL) v1.0.

2 Measurement sites and their characteristics

The data used here concern an area in and around the Landes forest in south-western France, in vicinity of the Atlantic coast. Detailed measurements were taken during the summer of 2017 (LANDEX episode 1) in an observation site located at Salles-Bilos, the exact period of the measurements being from 20/06/2017 to 20/07/2017. More information about this site is given in the next section.

Additionally, 10 air quality monitoring sites – from the ATMO national network - located around the forest have been used for validation of more common species (NO_x, PM_{10}, $PM_{2.5}$, Figure 1). Meteorological fields (explained in detail in section 3.3) used in the simulations have been validated using the E-OBS database as well as the data provided by the measurement site at Salles-Bilos.

2.1 Characteristics of the main measurements site and measurements performed

The measurements site is located at Salles-Bilos (44°29'39.69"N, 0°57'21.75"W, 37 m a.s.l), about 50 km in the south west of Bordeaux. It is located in the middle of the Landes forest (Figure 1), a large forest with a majority of maritime pine (Pinus

Table 1. Summary of changes in each test case. Each change has been explained in more detail in sections 3.1 through 3.6. Treetype/EF column refers to changes in tree type inputs and their respective emission factors. The wind/swrd/K_z column refers to the test case in which the inside canopy wind speed, short wave radiation, and vertical exchange coefficient parameters are modified. For each case the section in which the changes have been explained is mentioned in the first column.

Simulations	**Meteorology**	**landcover**	**MEGAN**	**Treetype/EF**	**Anthropogenic inputs**	**wind/swrd/Kz**
Base simulations (section 3.2)	WRF	Globcover	MEGANv2.1	Not included	EMEP 10 km×10 km	Not included
Case 1 (section 3.3)	ECMWF	Globcover	MEGANv2.1	Not included	EMEP 10 km×10 km	Not included
Case 2 (section 3.4)	ECMWF	Theia 2018	MEGANv3	Not included	EMEP 10 km×10 km	Not included
Case 3 (section 3.4)	ECMWF	Theia 2018	MEGANv3	Included	EMEP 10 km×10 km	Not included
Case 4 (section 3.5)	ECMWF	Theia 2018	MEGANv3	Included	ATMO-NA 1 km×1 km	Not included
Case 5 (section 3.6)	ECMWF	Theia 2018	MEGANv3	Included	ATMO-NA 1 km×1 km	Included

pinaster) trees. The forest parcels are intermittent with agricultural fields, and their affectation can change from year to year. The specific parcel where the measurements took place consists of pine trees planted in 2004. The height of the trees was around 10m in 2017. Regarding biogenic emissions, the site is quite homogeneous regarding tree types since the large majority of the trees in the surrounding area are maritime pines. However, as mentioned above, since the forest is parcellated, the density of the forest and the geographical distribution of these emissions have a certain degree of heterogeneity; parcels can become agricultural fields or replanted with pine trees, resulting in pine trees with different ages.

The intensive field campaign was carried out just next to the Salles-Bilos ICOS station, part of the European ecosystem monitoring network, where detailed measurements of greenhouse gases and meteorological parameters are obtained at 15m above ground on a measurement tower above the forest canopy (ICOS (2023); Moreaux et al. (2011)). During the LANDEX campaign, a large set of gaseous and aerosol measurements was added inside the forest canopy, at 6 m height (Bsaibes et al. (2020); Mermet et al. (2021)). For the purpose of this study, among gaseous species the measurements of O_3, nitrogen oxides (NO_x) and biogenic volatile organic compounds ($BVOC$s) will be used, and among the particulate compounds, the concentrations of PM_{10}, $PM_{2.5}$ and organic aerosols will be considered. A summary of the measurements used at this site is shown in Figure 1.

O_3 measurements were performed inside the forest canopy, with the APOA-370 (HORIBA) UV absorption instrument using a temporal resolution of 5 minutes.

NO and NO_2 measurements were performed by chemiluminescence, using an APNA 370 (HORIBA) with a resolution of 5 minutes and the same height as the O_3 measurements. This measurement method being not specific for NO_2, resulting NO_2 measurements may be overestimated especially for background conditions when much of the concentration of NO_y species are oxidized.

VOCs were measured with an ensemble of different instruments (Mermet et al. (2019), Bsaibes et al. (2020), Mermet et al. (2021)). A PTR-Tof-MS (Proton Transfer – Time of Flight – Mass Spectrometer) allowed to measure the total concentration of terpenoids (isoprene, mono and sesquiterpenes) below the forest canopy at the same height as the previous measurements (around 6 m). Another PTR-Tof-MS was utilized for measurements above the canopy (results for these measurements were not available to this author). In addition, GC-MS measurements were also performed for characterizing $BVOC$ speciation. In this work, the sum of the terpene species resulting from these measurements as well as the individual concentrations of α-pinene, β-pinene, limonene and ocimene are used. Since the purpose of the article is to focus on organic aerosol formation from biogenic compounds and the effect of anthropogenic VOCs in the atmospheric chemistry of region is limited, anthropogenic VOC measurements are not explored.

Attempts to measure radical species were also made, specifically for OH (using a FAGE instrument from the PC2A partner; Amedro et al. (2012)) and NO_3 (IBBCEAS technique from the LISA laboratory – University Paris-Est Creteil, Fouqueau et al. (2020)). Because of technical problems, the measurements for OH were not available to be used in this paper. The observed NO_3 concentrations were too low to produce a detectable signal on the instrument; therefore they were considered to be below the detection limit of the instrument, therefore below 3-5 pptv.

Particulate matter was also measured during the campaign. PM_{10}/$PM_{2.5}$/PM_1 concentrations were measured using a traditional TEOM-FDMS microbalance (implemented by EPOC) and a FIDAS 200 analyzer (deployed by INERIS), which measures total aerosol concentration in the range of 0.18 - 100 μm (with 3 measuring ranges). INERIS also utilized an aethalometer at the same time as the FIDAS in order to measure the black carbon (BC) concentrations. They identified a strong biomass burning episode (on the 05/07 to 06/07) near the measurement site, producing a peak of BC with concentrations as high as 80 $\mu g.m^{-3}$. The simulation of fire episodes using inputs from satellite data is implemented in CHIMERE, but this option was not activated for the runs performed in this study. Therefore, and since SOA build-up from biomass burning is not the aim of this paper, this peak has been removed from the PM data produced by the FIDAS.

A high-resolution time-of-flight AMS (HR-ToF-AMS, Aerodyne Research Inc.; DeCarlo et al. (2006)) was used in order to measure the bulk chemical composition of the non-refractory fraction of the aerosol operated under standard conditions (i.e., temperature of the vaporizer set at 600 °C, electronic ionization (EI) at 70 eV) with a temporal resolution of 8 minutes. The concentration of organic aerosol in the PM_1 fraction resulting from this instrument is used in this study.

It should be mentioned that all the measurements used in this work were performed inside canopy, except meteorological parameters, which were measured both inside and above the canopy. For meteorological parameters the above canopy measurements have been used.

2.2 Other measurement data

The latest version of the E-OBS dataset (Cornes et al., 2018) was used for large-scale meteorological validations, for the European and the French domains (see Figure SI-1). These data provide daily regridded information for temperature (daily average, minimum and maximum), wind speed and direction, relative humidity, precipitation, and solar radiation for around 5000 stations for temperature related variables and around 1800 for other parameters covering the current day period going back to 1950s. The data can be downloaded in a regridded format (with a $0.25^\circ \times 0.25^\circ$ horizontal resolution) or point data (as in the data for each station); the second option is used in this study.

For more comparisons, data from 10 air quality monitoring stations from the ATMO network were also included. The location of these stations, generally at the edge of the forest, is shown in Figure 1. The measurements available for most of these stations include nitrogen oxides (NO and NO_2) and PM (PM_{10} and $PM_{2.5}$) mass concentrations. These datasets were provided by the local air quality monitoring agency, the ATMO-NA (Atmo-Nouvelle-Aquitaine (2023)), information on the instruments used for the measurements is provided on their site and historic data is provided upon request. The data covers the entire period of the campaign.

3 The modeling chain

In this section, the reference simulation and sensitivity tests will be presented in detail, in each case documenting the choices made for the changes. The parameters common to all sensitivity tests are explained in section 3.1. After the description of the base simulation (section 3.2), sections 3.3 through 3.6 describe sensitivity tests changing inputs/variable calculations. Keep in mind that each modification is added on top of the previous ones. The implemented changes are indicated in Table 1.

3.1 CHIMERE chemistry transport model

The CHIMERE offline regional chemistry transport model (Menut et al., 2013) was developed initially in the early 2000s in order to simulate the concentrations of gaseous species (especially O_3). Later on, a module for the simulation of particulate matter (Pun and Seigneur (2007); Bessagnet et al. (2008)) was added to the model. The model is currently used extensively in air quality monitoring and forecast in research as well as for operative purposes both in regional and hemispheric levels (Cholakian et al. (2019b); Lachatre et al. (2019); Trewhela et al. (2019); Lapere et al. (2020)). It has also been used in many model intercomparison studies, as well as model-observation comparisons within multi-model experiments, for example to investigate European particulate matter trends (Ciarelli et al., 2019). Mandatory input information includes meteorological fields, landcover parameters, biogenic/anthropogenic emissions factors and boundary/limit conditions. Having access to this data, CHIMERE then simulates 3D concentration and deposition fields for a list of gaseous and size resolved particulate species, depending on the selected chemical scheme. In this study, the 2017 version of the model has been used (Mailler et al., 2017). In the following section, information about the reference parametrization is provided.

3.2 Base case simulation

The simulations conducted in this study were performed on 3 domains: a continental domain with a horizontal resolution of 25 km, covering the whole Europe and the northern Africa (Figure SI-1), an intermediary nested domain focused on France with a horizontal resolution of 5 km (Figure SI-1) and a 1 km horizontal resolution domain focused on the Landes forest nested inside the intermediary domain (Figure 1). The vertical resolution of the simulations is the same for each domain, 15 levels starting from 13 m to about 12 km (a.s.l.). Only for the canopy parametrization case (section 3.6) vertical levels were modified. The simulations were performed for the period of 01-06-2017 to 20-07-2017, with a spin-up period of 5 days.

The SAPRC-07A (Carter, 2010) chemical scheme has been used for all the simulations since it provides more details for the terpenoid oxidation than the previously used Melchior scheme. The aerosol size bins are the same for all simulations, a 10-bin logarithmic sectional distribution in a range of 40 nm to 40 μm; the chemical speciation of aerosols contains EC (elemental carbon), nitrates (NO_3^-), sulfates (SO_4^{2-}), ammonium (NH_4^+), primary organic aerosols (POA) and secondary organic aerosols (SOAs), dust, sea salt and PPM (Primary mineral Particulate Matter except the ones mentioned above).

The selected SOA scheme allows differentiating between about 10 surrogate species of semi-volatile $BVOC$ oxidation products with different composition, volatility, and solubility and created in a single oxidation step (Pun and Seigneur (2007); Bessagnet et al. (2008)). It takes into account initial oxidant attack from OH, O_3 and NO_3. The scheme has been used and evaluated in multiple occasions (Lemaire et al. (2016); Cholakian et al. (2018); Cholakian et al. (2019a)). Since this study relies heavily on SOA formation and comparison of this species to measurements, a brief introduction of this scheme will be provided here. The scheme is based on Odum et al. (1996), a simple two-product scheme with the advantage of being numerically light. In this scheme it is considered that the oxidation of BVOCs results in the formation of semi-volatile products with a yield specific to each BVOC family. Some BVOCs consist of specific species (isoprene, α-pinene, β-pinene), others are surrogate groups consisting of similar species lumped together (ocimene, limonene, sesqui-terpenes, etc.). As mentioned above, it considers only one step of oxidation for the BVOCs. Assuming homogeneous mixture, Raoult's law is applied combined with the Pankow theorem (Pankow, 1987) resulting in the calculation of the SOA production yield. The scheme is explained in more detail in Pun and Seigneur (2007). The oxidation reactions that are applied for the production of semi-volatile VOCs have been updated in order to take into account more recent (and more detailed) reactions and reaction rates. The values given on the Carter (2019) site (following Carter (2010)) were used in order to update the reaction rate constants of the BVOCs mentioned above with OH, O_3 and NO_3. The SOA yields have been kept the same as what is provided in Pun and Seigneur (2007) and Bessagnet et al. (2008) as well as provided in the CHIMERE (2023) documentation. We have also added the reactions of $BVOC$s with different oxidants in the SI (refer to SI-8).

Boundary/initial conditions are taken from climatological simulations of LMDz-INCA3 (Hauglustaine et al., 2014) for gaseous and particulate species and GOCART (Chin et al., 2002) for dust concentrations.

For each CHIMERE simulation domain, the meteorological parameters were obtained by running the WRF model (version 3.9.1.1; Wang et al. (2015)) on the same domain and with the same horizontal resolution with the NCEP large-scale input data (for Environmental Prediction/National Weather Service/NOAA/US Department of Commerce, 2000). Several model

configurations have been tested for WRF. A comparison of the model outputs with the E-OBS database (Cornes et al., 2018) and with the measurements obtained at the Salles-Bilos measurement site was conducted for all the performed meteorological runs. For the base simulations, the WRF configuration showing the best comparison results (as detailed in the SI-2) with the Salles-Bilos site was chosen (see Figure 2 for time series and statistical information). All the parametrizations tested for WRF are presented in SI-2. The WRF parametrization that is retained is a two-way triple nested run with WSM 6-class graupel microphysics scheme, Kain-Fritsch cumulus scheme, RRTMG scheme for both shortwave and longwave radiation, Noah-MP land-surface, MYNN surface layer option, MYNN 3^{rd} level TKE boundary layer height option, topological wind, urban physics and lake physics options and nudging options activated. These options are all described in detail in the user guide for the Weather Research and Forecast (WRF) model (Wang et al., 2015).

The Globcover (Arino et al., 2008) dataset with a resolution of 300 m$\times$300 m was used for the landcover parameters. Bearing in mind that the forest is parcellated and that some parcels can be transformed into agricultural fields, changing this database to a more recent one was considered to be beneficial for this study (see 3.4).

Biogenic emissions are provided by a reduced online version of the MEGAN (Guenther et al., 2012) model already having been integrated in the CHIMERE model. For the base simulations the version 2.1 of the MEGAN model has been used. This version of MEGAN comes with pre-calculated $BVOC$ emission factors for isoprene, α-pinene, β-pinene, limonene, ocimene, humulene and β-caryophyllene (also including the leaf area index (LAI) fields) with a horizontal resolution of 0.008 $^\circ \times$ 0.008°. Therefore, any landcover related changes in the model will not affect the $BVOC$ emission factors. These emission factors were calculated using the Globcover landcover database. In a later sensitivity test (section 3.4), a more recent version of the MEGAN model has been tested. Using this version, we have the possibility of recalculating the $BVOC$ emission factors by changing the landcover, the vegetation-specific emission factors and the LAI. A more detailed explanation of this model and its use is provided in section 3.4.

Anthropogenic emissions were taken from the EMEP (EEA) emission database with a 10 km resolution for the year 2014. The emissions in this database for the years 2014, 2016 and 2017 were compared and no major differences were observed in the levels of anthropogenic emissions between these years for this specific region (the data can be directly compared on the EMEP emissions datacenter accessible here: EMEP (2023)). The reason for using the 2014 emissions is explained in detail in section 3.5, where a local high resolution emission database is tested.

It is worth mentioning here that the CHIMERE model does not have an integrated forest canopy model; therefore, the model, while taking into account the biogenic emissions and the landcover information of the forest in different modules (for example for calculating the deposition of atmospheric species), will not take into account the dynamic physical changes introduced by the forest canopy into the concentrations of chemical species in the first two vertical layers of the simulations. These effects and the changes made in the model in order to address them are presented in detail in section 3.6.

3.3 Meteorological inputs

In addition to the tested WRF parametrizations, another series of meteorological inputs was tested using the ECMWF high-resolution 3 hourly forecast dataset (Owens and Hewson, 2018). The global version of the ECMWF data (with lower resolution)

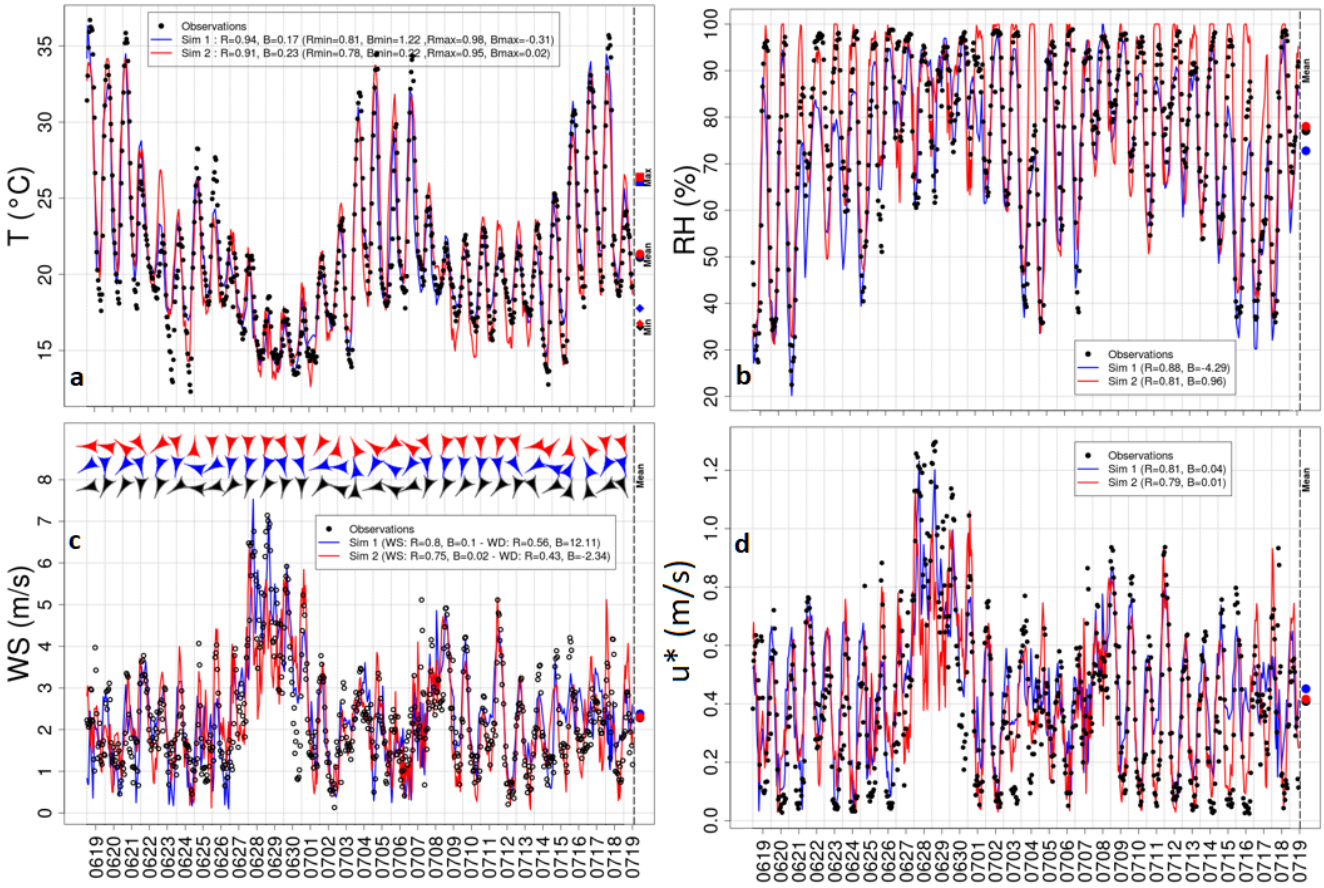

Figure 2. Meteorological comparisons for the 2 meteorological inputs: the blue series (SIM1) show the ECMWF simulations and the red ones (SIM2) the WRF outputs. Statistical information is provided in the legend for each figure (R correlation coefficient, B bias (simulation - observation)). The name of each parameter is written on the side of each panel, points on the right side of each panel showing the average data for each series. The comparisons are performed for the 1km domain and for the Salles-Bilos measurement site. The comparisons are performed on the surface level. Panels a through d show temperature (panel a, marked as T in °C), relative humidity (panel b, marked as RH, in %), wind speed and wind direction (both in panel c, Ws is wind speed in m/s, directions are shown on top of each day) and friction velocity (panel d, marked as u* in $m.s^{-1}$) respectively. More information about all the WRF simulations and the one that was chosen to be presented here (noted as WRF3) has been shown in SI-2.

is used for the continental domain, while for the other two domains the high-resolution (10 km) ECMWF run is used. The comparisons of the measurements from the Salles-Bilos site to a simulation run with the ECMWF meteorological inputs is shown in Figure 2, as well as the comparison for the WRF parametrization mentioned in section 3.2. Before commenting on this comparison, we first briefly present the meteorological situation during the campaign which is depicted by both models in a similar way. Rainfall events (not shown in Figure 2) occurred between June the 26^{th} and July the 3^{rd} and also in the July

8^{th} to 13^{th} 2017 period and were associated with low solar irradiance (< 750 W.m^{-2}), mild summer temperatures (< 25 $^{\circ}C$), high relative humidity (> 75%) and moderate winds. These periods are defined as "low oxidation" periods. Two episodes of sunny conditions were observed during the campaign, i.e. from July the 4^{th} to the 7^{th} then from the 14^{th} to the 18^{th}. These periods were characterized by higher temperatures, relative humidity below 50% (during the day), low wind speeds (< 3 m.s^{-1}) and friction velocity (< 0.3 m.s^{-1}) and no precipitation. These periods were favorable to plant emissions and strong oxidant formation and are called periods of "strong oxidation". It appears that models adequately describe the broad meteorological situation during the campaign summarized by Mermet et al. (2021).

While both meteorological runs here represent the measurements site on the smallest domain quite accurately, the ECMWF run shows a better representation for the two bigger domains for all the tested parameters (mean, maximum and minimum temperature, wind speed and direction and relative humidity, see SI-2), thus providing more accurate meteorological patterns at the boundaries of the high-resolution domain. As for the high-resolution domain, the daily mean and maximum temperature values are well simulated in both meteorological inputs (Figure 2, panel a). However, both models have shortcomings in the representation of daily minimum temperature values: this problem is more significant in the WRF simulations (on daily minima, a bias (simulation - observation) of +0.22$^{\circ}C$ and +1.22$^{\circ}C$ is observed in the ECMWF and WRF data respectively). The wind speed simulations are accurate in both runs (Figure 2, panel c), while the wind direction is more representative of the domain in the ECMWF simulations. The friction velocity (u*, Figure 2, panel d) shows the same pattern and is well represented in both datasets, although the night-time minimum is better represented in the WRF simulations. Precipitation and the Bowen ratio β (the ratio of heat flux to moisture flux near the surface) were also compared, and are presented in SI-3.

3.4 landcover, tree type and tree-specific emission factors

Since the forest is parcellated and goes through annual changes, it is important to use an up-to-date source of information on forest cover and density when performing high resolution simulations. To this end, a detailed comparison of existing landcover data was conducted. It should be noted that, in most landcover databases, trees are lumped in two main functional groups: broadleaf and needleleaf trees. In addition to tree density (which varies upon the selected database), the broadleaf/needleleaf distribution is also a specific parameter of a landcover datasets. This is why, in this exercise, all databases have been examined with regard to their total tree density (this section), but also with respect to the $BVOC$ emissions they induce, with respect to the broadleaf/needleleaf distribution (next section).

In particular, from this section on, a more recent version of MEGAN (MEGAN3.0, Guenther et al. (2018)) has been used, which provides the possibility to modify the landcover and the emission factors attached to different tree types and different regions. Therefore, all the modifications mentioned in this section were made both in MEGAN and in CHIMERE simultaneously. We performed two separate test cases in this section: one for changing the landcover data and the second for changing the regional tree species and the emission factors tied to specific trees. Both these modifications result in changes in the general $BVOC$ emission factors; therefore, they are presented in the same section.

In the first test case, we considered the datasets provided by CHIMERE and WRF models and compared them to several other more recent or regionally specific datasets. CHIMERE allows the use of two datasets for landcover information: the

Globcover dataset (Arino et al., 2008) as selected for the base simulation, and the USGS dataset (Gutman et al., 2008). As for the WRF model, it provides the option of using MODIS (Giri et al., 2005) or USGS data. Also, the forest cover density information made available in MEGAN was also included in our comparisons. In addition to these data, three databases of major interest were added to our comparison (panels b, c and d of Figure 3).

First, we considered the Copernicus database (Copernicus, 2023), which provides (among other parameters) information about the tree cover density over Europe for the years 2012 and 2015 with a horizontal resolution of 20 m. The Copernicus database also provides forest changes across Europe between the years 2012 and 2015. These changes are, on the average, about +30% forest growth in grid cells where the changes were positive and about -40% in grid cells where the changes were negative. Given these important changes, only the most recent (2015) dataset was considered. This database was regridded to our 1km resolution domain to have a common grid for comparisons (panel e of Figure 3).

We also collected data from the IGN (Institut national de l'information géographique et forestière) which provides detailed information on forest density (via the BDForêt database) and on general landcover information (via the BDTopo database) in France. These data were downloaded from the IGN data portal (IGN, 2023a) for three administrative departments (Landes (40), Gironde (33) and Lot et Garonne (47)) in order to cover the entire Landes forest. Both the BDForêt and the BDTopo databases have high resolution (around 20 m); temporally, the BDTopo database is for the year 2017 (pubished in 2019) while the BDForêt database was updated in the year 2018 with data from the year 2017. The data for both databases were processed into a format that is usable in CHIMERE (i.e. projection of shapefiles onto a regular netcdf grid) and then regridded to the 1 km domain. This provides us with two more sources of comparison shown in Figure 3 (panels f and g, noted as BDForêt and BDTopo).

There is also a landcover dataset provided by the French national institute of agriculture, alimentation, and environment (INRAE, Institut national de recherche pour l'agriculture, l'alimentation et l'environnement), called the Theia dataset (IGN, 2023b). This dataset includes several types (reflectance, snow mask, water level, etc.) of information gained from remote sensing observations of the earth, including landcover data. The dataset was realized first in 2016, then updated in 2018, with a horizontal resolution of 20 m. Both datasets for years 2016 and 2018 are presented in this study (Figure 3, panels a and h). It is important to know that the base data used in order to generate the Theia datasets, apart from satellite information is the BDTopo database presented in the previous paragraph. Comparing the two Theia datasets (2016 and 2018) a difference of 29% is seen when conifers tree density is involved (although differences in total tree cover are small, see below).

Since Theia-2018 is the most recent source of information we could acquire for the region at this time and since it is based on several independent data sources, it was taken as reference in Figure 3, panel a. The upper left frame shows the 2018 Theia tree cover density for the Landes forest in shades of green. It draws a strongly delimited triangle of dense forested area on the domain, which becomes irregular in the southern part of the domain and near the coastline. The other frames show the relative difference of each database with respect to Theia-2018. It can be seen that there are practically no differences between Theia-2018, BDTopo and Theia-2016 (average density over the forest is respectively 68.32%, 68.95% and 68.20%), and only slightly lower densities in the BDForêt and MEGAN databases (63.2% and 58.29% respectively), while strong differences appear with the MODIS, Globcover, Copernicus and USGS data. MODIS proposes a much higher forest density than Theia, especially in

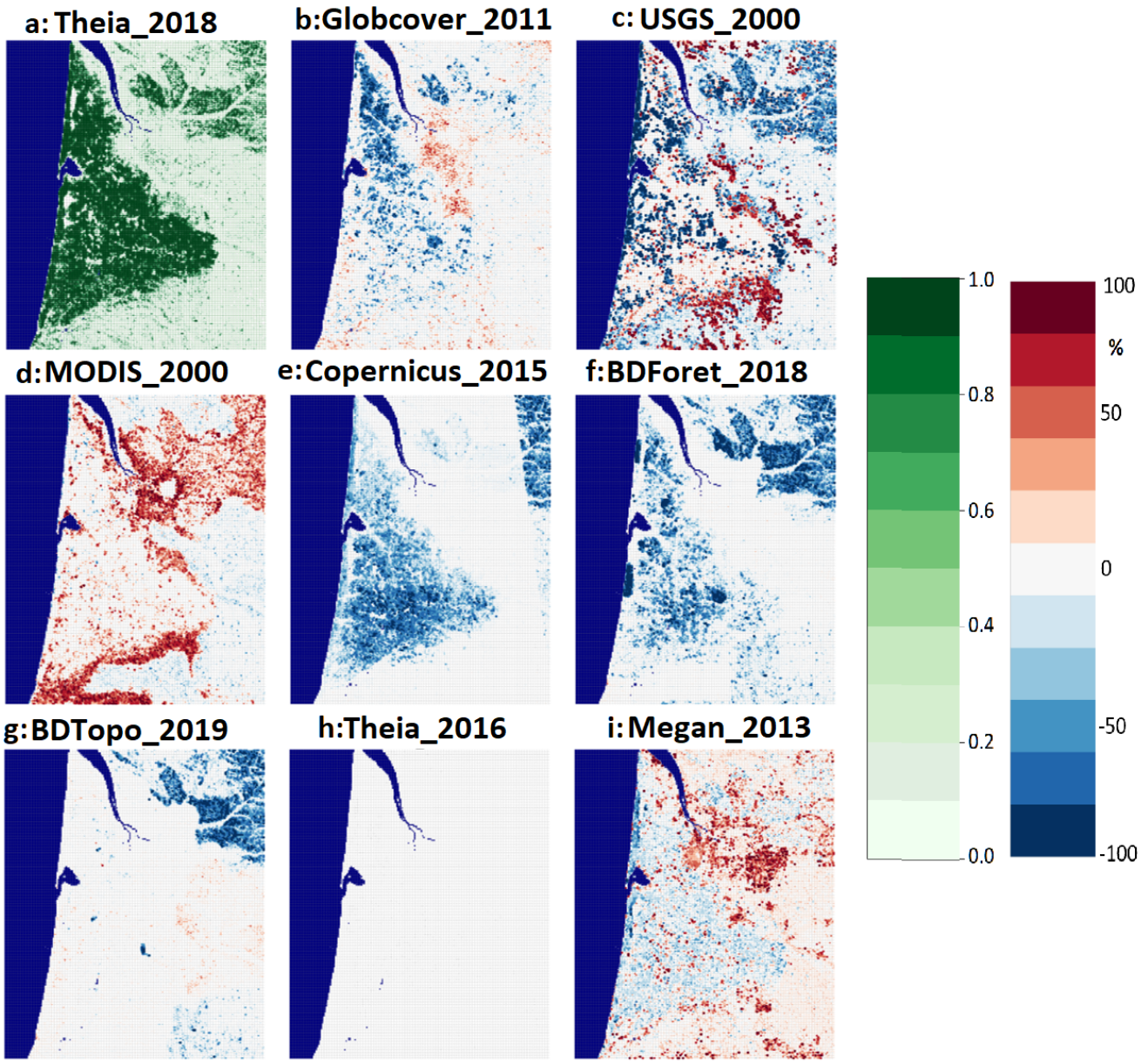

Figure 3. Forest density comparisons for different landcover databases: name of each database is shown on top of each image. The forest density is shown for the Theia2018 dataset on the first panel, the rest of the images show the percentage differences between each database with the Theia2018 dataset. Two scales are provided for the figure; the first scale (shades of green) corresponds to the reference case (panel a), the second scale shows differences of each panel to the reference case (panels b through i).

and around the edge of the Landes forest. A possible reason for this could be the data being outdated (the MODIS version used here dates from 2000) or the lower resolution of MODIS (1 km×1 km) compared to the others. The Copernicus database

shows a consistent underestimation of the forested area over the Landes forest. Same is true for the Globcover database to a lesser degree; probably because its resolution is higher than MODIS, but it is still outdated (2000s). The USGS database shows either a strong overestimation or an underestimation for different 1km grid cells. Since this database is quite old (2003), the changes between forest and agricultural fields could be responsible for these discrepancies. From this point on, the Theia-2018 landcover database has been used both in CHIMERE and in MEGAN.

The second step in this section is to analyze the estimation of the $BVOC$ emission factors when tree types in the region and tree-specific emission factors are changed in MEGAN. The BDForêt database mentioned above provides more detailed information about distribution of tree species inside the Landes forest as well as their density. It was considered necessary to modify the tree type distribution in the MEGAN v3 model since originally it assumes 28% of maritime pine coverage for the Landes forest, while the BDForêt database shows around 95% of the same species. The reason for this discrepancy is that MEGAN considers an average tree species distribution for western European forests up to 300 km from the Atlantic coast, which does not take into account the specificity of the Landes forest. Therefore, modifications were made in the MEGAN v3 model inputs in order to i) create a specific ecosystem for the Landes forest containing 95% of maritime pines and ii) modify the emission factors for the maritime pine to experimental values obtained during the Landex campaign (E. Ormeno, personal communication). The emission factor for maritime pines was measured on the canopy and also on the litter levels during the same campaign this study simulates. The measurements resulted in an average of 3.8 $\mu g.g^{-1}.h^{-1}$ at the canopy level and an average of 1.6 $mg.g^{-1}.h^{-1}$ at the litter level of total monoterpene emissions (individual emission factors for BVOCs are also available upon request from the source mentioned in the article). The values provided here for the canopy and the litter are respectively almost 3 times and 2 times higher respectively than the original values used in MEGAN v3. The resulting emission factors were integrated into MEGAN v3. Total emission factors per $BVOC$ were generted and integrated in CHIMERE and a sensitivity case was run with this new configuration. The resulting emissions of isoprene and the sum of terpenoids (mono and sesqui terpenes) using these new emission factors are shown in Figure 4 for both sensitivity tests detailed in this section. Figure 4 justifies a posteriori the importance of this sensitivity test, since the emissions of isoprene have dropped by about half, while the emissions of terpenoids have increased significantly, by about a factor of 2. In Section 4.1, we will explore the effect of these emission changes on $BVOC$ concentrations and compare the results to observations. Taking into account that maritime pine is terpene-emitting and that the forest is mostly covered by these species, these emissions are more realistic for the Landes forest than the original ones. Monoterpene emissions (averaged over the entire forest) increase around 33% when only landcover is changed (Figure 4, panel b), while emissions of isoprene decrease by around 30% by landcover data change (Figure 4, panel e). For the region being studied here it is important to notice that the effect of changing the type of trees and the experimental emission factors for these trees is more important for the emission of monoterpenes, while the change caused by modifying the landcover seems to be more important for isoprene emissions.

It should be taken into account that, a test was run by replacing the LAI used in the model by the Copernicus 1 km horizontal resolution global LAI-v2 databases (Copernicus Land services, 2023) for the year 2017, leading to no significant changes in the results of the simulations compared to when the LAI implemented in CHIMERE (from MEGAN v3) is used.

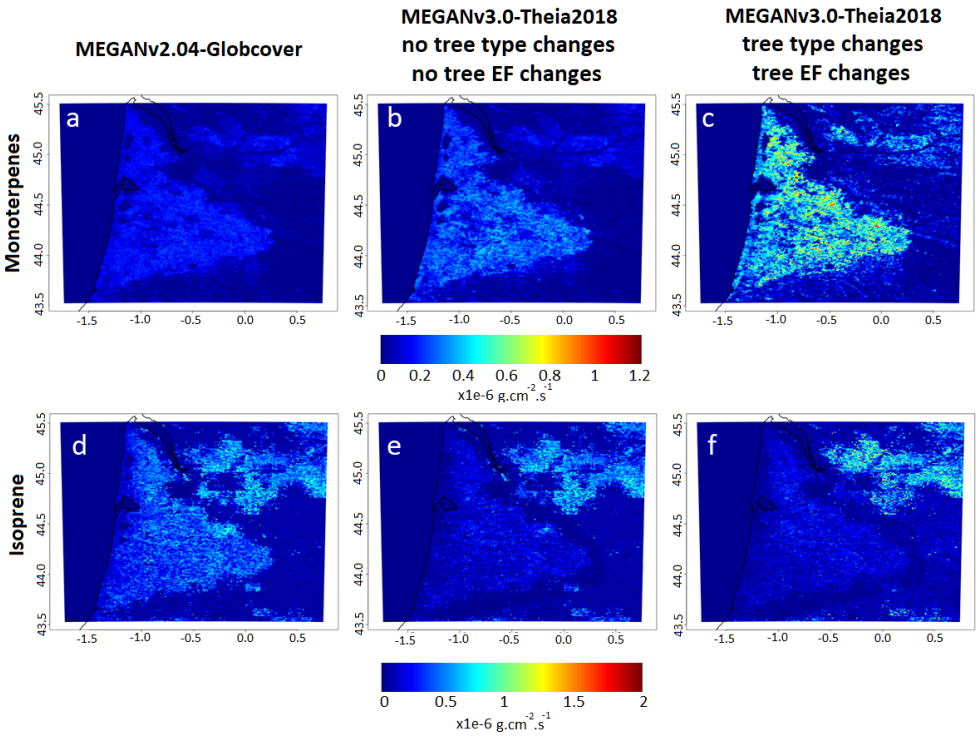

Figure 4. Changes to monoterpene (first row, panels a through c) and isoprene (second row, panels d through f) emissions in base case conditions (first column from the left, panels a and d), changing only the landcover (middle column, panels b and e) and when both landcover and MEGAN version are updated (third column from the left, panels c and f). For each species one scale is provided under the three panels, keep in mind both scales should be multiplied by $1e^{-6}$, the unit for all panels is $g.cm^{-1}.s^{-1}$.

3.5 Anthropogenic emissions

For the reference simulation, anthropogenic emissions from the EMEP inventory are used, with a horizontal resolution of 10 km. This is assumed to be precise enough because the region has, at least when it comes to the forest, a low anthropogenic footprint. However, the transport of recently emitted compounds to the forest by the anthropized areas around the forest (including large cities such as the Bordeaux metropole to the north and smaller ones such as Dax to the south, as well as industrial sites located to the west and northwest of the forest) as well as motorway traffic passing through the forest needs to be taken into account in more detail. To this end, we have implemented in CHIMERE the kilometric emission dataset provided by the regional air quality agency (ATMO-NA). This 5^{th} sensitivity case revolves around changing the anthropogenic emissions from the reference EMEP emissions to the emissions provided by ATMO-NA. This modification, in addition to providing anthropogenic emissions with greatly increased horizontal resolution, has the advantage of being prepared from bottom-up data specific to this area. The comparison of these two emission datasets is shown in SI-4. In summary, the two databases show comparable emissions for all species, presenting the highest average bias (simulation - observation) for SO_x of around 20%, dominant

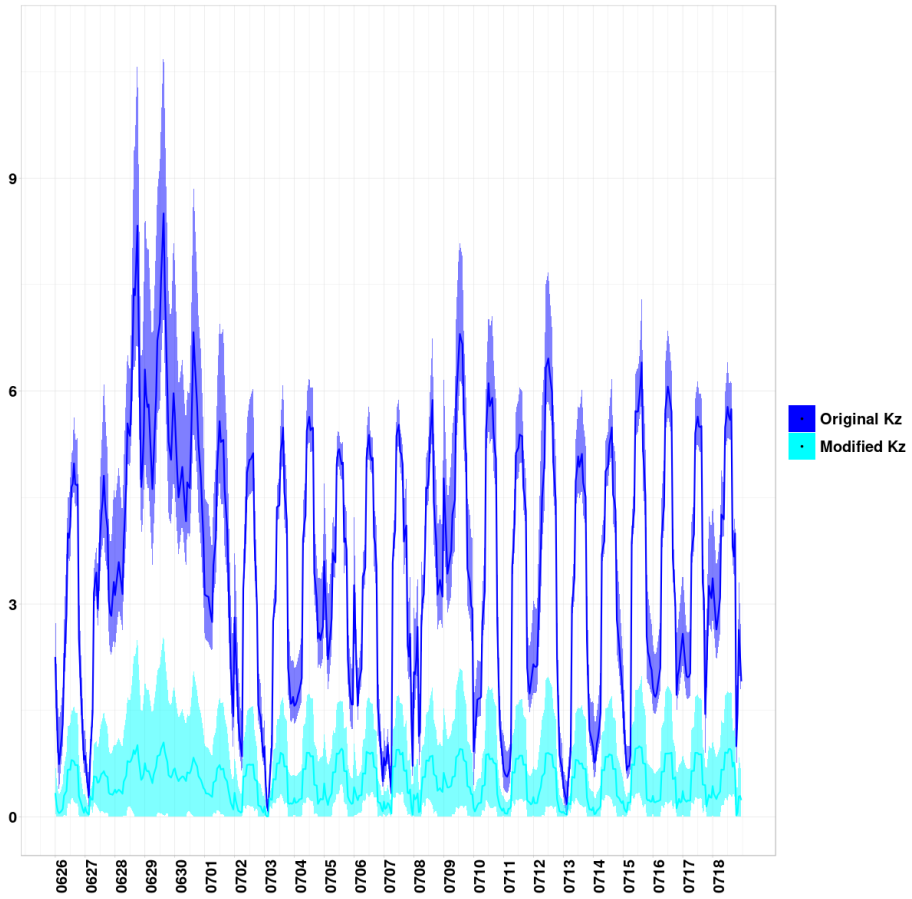

Figure 5. Changes in K_z ($m^2.s^{-1}$) between the first and second model layer in test cases without any modifications and the test case in which the K_z corrections are applied. The lines are for the grid cell corresponding to the Salles-Bilos site and the envelope corresponds to grid cells in the 11 km×11 km area around. The reasoning for showing 11 km×11 km is given later in section 4.

SNAP sectors being always the same for each species groups between the two emission inventories. It should be noted that the emissions provided by ATMO-NA are for the year 2014; therefore, in order to have consistent emission inventories, we have used the 2014 EMEP emission inventory for this test. For information, the total national NO_x emissions differ around 9% between 2014 and 2017 on average in the EMEP dataset.

3.6 Vertical diffusion, wind speed and shortwave radiation corrections

Since the CHIMERE model does not have a coupled canopy model, it cannot take into account the physical effects that the forest canopy might exert on concentrations of chemical species. The last sensitivity case is based on the corrections of the effects that the canopy can have on the simulation of the physical parameters such as vertical diffusion (K_z, $m^2.s^{-1}$), wind speed and shortwave radiation in the model (it will be referred as the final test case from here on).

While the effect of the canopy on $BVOC$ emissions is already taken into account in the MEGAN model, the effects of the canopy on wind speed and vertical diffusion inside the forest are not simulated in the CHIMERE model. On a large-scale simulation and not comparing to inside-canopy measurements this usually does not cause major issues. But since the goal of this work was to understand the atmospheric situation inside the canopy, almost all measurements are performed inside it. Furthermore, simulations performed here are high resolution simulations, therefore, we have added corrections for the aforementioned physical parameters inside the canopy in order to simulate the physical conditions of the forest more realistically. These modifications will be presented as the 6^{th} sensitivity test, theoretically thought to be the most realistic one. In this test, a small inconsistency subsists because deposition is only treated in the lowest layer in the model, while it also could affect the second layer which contains part of the canopy.

For this purpose, the vertical diffusion and the wind speed correction suggested by Ogée et al. (2003) and Leuning (2000) implemented within the MUSICA canopy model have been integrated into the fine domain of our simulation for the model grid cells where the forest density is higher than 70%. The MUSICA canopy model is a 1D model developed in the early 2000s; it has been detailed by Ogée et al. (2003). The case study presented in the aforementioned study is also for the Landes forest and has been validated by comparisons against measurements.

In the standard version of the CHIMERE model, the vertical diffusion (K_z) is calculated by the parametrization suggested by Troen and Mahrt (1986). Depending on the atmospheric stability (determined by the Monin-Obukov length), the K_z can relate to u* in different ways depending on atmospheric stability. The equation for K_z is:

$$K_z = k w_s \frac{z}{h}(1-\frac{z}{h})^2 \tag{1}$$

Where k represents the von Kármán constant and the factor w_s is calculated differently depending on the atmospheric stability:

$$\text{Stable conditions} : w_s = \frac{u_*}{(1+4.7\frac{z}{L}))} \tag{2}$$

$$\text{Unstable conditions} : w_s = (u_*^3 + 2.8 e w_*^3)^{\frac{1}{3}} \tag{3}$$

Where, $\frac{z}{L}$ is the ratio of altitude to height of the boundary layer, u_* is the friction velocity and L is the Monin-obukov length. More explanation on the calculation of K_z can be found in the Chimere model documentation (downloadable from CHIMERE (2023) site.).

In this work we have added the diffusivity and horizontal wind correction factors ($\phi_w(\xi)$ and $\phi_h(\xi)$ respectively) using the references mentioned above:

$$\phi_w(\xi) = \begin{cases} 1.25(1+3\,|\xi|)^{-\frac{1}{3}}, -2 \leqslant \xi < 0 \\ 1.25(1+0.2\xi), 0 \leqslant \xi < 1 \end{cases} \tag{4}$$

$$\phi_h(\xi) = \begin{cases} (1+16\,|\xi|)^{-\frac{1}{2}}, -2 \leqslant \xi < 0 \\ (1+5\xi), 0 \leqslant \xi < 1 \end{cases} \tag{5}$$

Where, ξ the stability factor is calculated by:

$$\xi = \begin{cases} \frac{h_c}{L}, z < z_{ruf} \\ \frac{(z-d)}{L}, z \geq z_{ruf} \end{cases} \tag{6}$$

Where, h_c is the canopy height (m), z is the altitude (m), d is the zero-plane displacement for momentum and $z_ruf \approx 2.3h_c$.

410 In the end, the K_z is calculated by the following equation taking into account the diffusivity correction:

$$K_z = \phi_w k w_s \frac{z}{h}(1-\frac{z}{h})^2 \tag{7}$$

And the horizontal wind speed components are multiplied by ϕ_h. The diffusion and wind corrections are affected only to the first level of the model, which has a height of 8 m specifically for this case, and for grid cells with a forest density greater than 70%; a stability correction is also included at the same time (explained in Ogée et al. (2003)).

415 The changes induced for the vertical diffusion are shown in Figure 5. The line shows the K_z in the measurement site, and the ribbon around the line shows the regional changes around the measurement site up to a distance of 5 km on each side. The upper panel shows the standard vertical diffusion and the lower one the corrected K_z. Results indicate a strong decrease, by roughly one order of magnitude in the vertical exchange coefficient between the first and second model layer, when the canopy parametrization is taken into account.

420 The modification for shortwave radiation penetration inside the canopy comes from Hassika et al. (1997), which itself is a continuation of the work performed by Berbigier and Bonnefond (1995). Both studies revolve around the Landes forest, yet are general in their formulation. The following variation of Beer's law is used to achieve this purpose:

$$swrd(z) = swrd(0)e^{\frac{-k \times LAI(z)}{cos\beta}} \tag{8}$$

where $swrd(z)$ is the shortwave direct radiation at the altitude z, $swrd(0)$ is the shortwave direct radiation above canopy
425 level, $LAI(\lambda)$ is the leaf area index at the altitude z, β is the zenithal angle and lastly k is an extinction factor, which was measured to be 0.33 for the Landes forest (calculated by Ogée et al. (2003) using experimental data). In the case of our simulation, we do not need a distribution of shortwave radiation for different altitudes within the canopy, but rather a bulk decrease that we calculate here for the middle of the lower part of the first model layer between 0 to 6 m height (because LAI is supposed to be distributed between 6 and 10 m above ground level). This simulated value can thus be observed at 6 m height
430 at Salles-Bilos. According to visual inspection of the measurement site, most of the LAI is distributed in the last meters of the pine trees in that specific patch of the forest. This equation is also used on grid cells with higher than 70% tree density. It is also

important to take into account that the swrd changes affect only the chemistry modules of the model, by reducing photolysis frequencies. On the contrary, emissions of $BVOC$s are not affected by these modifications, since the effect of the canopy on the decrease of swrd is already taken into account in the MEGAN model when calculating the $BVOC$ emission factors.

These modifications were added in 2 steps: first the K_z and the wind speed modifications and second the swrd modification. Therefore, it was possible to determine the changes made by K_z/wind speed modifications compared to the changes induced by the swrd changes. The changes made to the K_z before and after the correction are shown in Figure 5.

It is important to keep in mind that this modification has been performed as a sensitivity case and not a functional parametrization for the model. The correction factors for diffusivity and wind speed have been calculated for this measurement site according to the work from Ogée et al. (2003). While they should be usable in other forests, the specific values should be adjusted to the specific conditions there (canopy height and LAI, especially). Also, canopy induced modifications in the vertical diffusion are considered at the top of the first model layer fixed for this case at 8 m height, so still well within the canopy (of 10 m height at the measurement site). For the wind speed and radiation, modifications are considered for the middle of the first layer, so at 4 m height.

4 Effects of the model configuration on simulations of SOA, precursors and oxidants

In this section, results from a series of sensitivity cases will be discussed, starting from a regional standard configuration of the CHIMERE model and moving to one updated for the local landes forest conditions. First primary gaseous species of biogenic and anthropogenic origins will be examined (section 4.1), then O_3 as a secondary species (section 4.2), radicals (section 4.3), and finally particulate matter with a focus on its organic fraction (section 4.4). Changes induced by sensitivity tests will be compared to measurements at the Salles-Bilos site. In section 4.5, the changes to the contribution of precursors and oxidants to $BSOA$ formation will be assessed in the base case compared to the simulation with all the modifications. Keep in mind that whenever changes are discussed in this section, changes of averages over the entire period of each test case compared to average of the entire period of the base case are being discussed.

Several of the species being discussed in the following sections have high local sensitivity depending on the forest coverage of a given location. As it is not clear, if the 1 km$\times$1 km model grid cell corresponding to the Salles-Bilos measurement site exactly matches local conditions, the range of simulated concentrations in a 11 km$\times$11 km square around the site will also be displayed.

In sections 4.1 to 4.4, observed and simulated time series at the Salles-Bilos site will first be analyzed. The percentage change of the concentration of different species caused by each sensitivity test compared to the previous one will be indicated. Finally, the effect of the complete set of sensitivity studies on their comparison to observations in terms of bias (simulation - observation), mean error and correlation will be addressed.

Table 2. Statistical information for test cases showing correlation coefficient to measurements (R, when possible), bias (absolute difference between model and measurement averages), minimum, maximum and average values (noted as min, max and mean), fraction of predictions within a factor of two of observations (FAC2), normalized mean bias (NMB) and the percentage of change of the mean for each test case compared to the base simulation. When measurement data was available, their value is given in parenthesis. The units and the species names are given on the left side of the table. %change indicates the relative change of simulated means with respect to the base case.

Species	Tests	R	Bias	Min	Max	Mean	FAC2	NMB	%change
NO_2 (ppb)	1:Base	0.43	-1.05	0.06(0.59)	5.75(12.17)	0.60(1.65)	0.22	-0.60	–
	2:1+meteo	0.56	-0.88	0.07	9.69	0.77	0.19	-0.50	29
	3:2+landcover	0.56	-0.89	0.07	10.08	0.76	0.18	-0.53	26
	4:3+megan	0.56	-0.91	0.07	9.91	0.74	0.18	-0.55	23
	5:4+emissions	0.59	-0.64	0.11	10.07	1.01	0.30	-0.35	68
	6:5+physical	0.61	-0.40	0.15	9.76	1.25	0.39	-0.31	109
O_3 (ppb)	1:Base	0.67	6.80	19.19(1.97)	57.73(62.08)	34.15(27.35)	0.81	0.18	–
	2:1+meteo	0.74	6.05	14.83	61.76	33.40	0.81	0.17	-2.2
	3:2+landcover	0.72	6.39	14.01	61.69	33.74	0.79	0.23	-1.2
	4:3+megan	0.72	6.25	13.09	60.85	33.60	0.79	0.23	-1.6
	5:4+emissions	0.73	6.35	13.00	68.29	33.70	0.79	0.23	-1.3
	6:5+physical	0.73	2.97	9.44	56.73	30.32	0.83	0.12	-11
Terpenes (ppb)	1:Base	0.30	-2.83	0.06(0.20)	1.93(24.86)	0.40(3.23)	0.49	-0.74	–
	2:1+meteo	0.28	-2.79	0.05	2.44	0.44	0.45	-0.77	11
	3:2+landcover	0.33	-2.64	0.07	3.82	0.59	0.43	-0.77	48
	4:3+megan	0.32	-1.89	0.15	9.13	1.34	0.62	-0.51	237
	5:4+emissions	0.31	-1.91	0.15	9.13	1.32	0.62	-0.51	231
	6:5+physical	0.31	-1.55	0.21	9.34	1.68	0.64	-0.11	322
OH (ppb)	1:Base	–	–	4.56×10^{-6}	2.88×10^{-3}	1.77×10^{-4}	–	–	–
	2:1+meteo	–	–	6.86×10^{-6}	3.46×10^{-3}	1.89×10^{-4}	–	–	6.6
	3:2+landcover	–	–	6.85×10^{-6}	2.08×10^{-3}	1.38×10^{-4}	–	–	-22
	4 :3+megan	–	–	6.23×10^{-6}	6.18×10^{-4}	6.61×10^{-5}	–	–	-63
	5:4+emissions	–	–	8.86×10^{-6}	5.17×10^{-4}	8.18×10^{-5}	–	–	-54
	6:5+physical	–	–	1.22×10^{-5}	3.88×10^{-4}	7.67×10^{-5}	–	–	-57
NO_3 (ppb)	1 :Base	–	–	1.88×10^{-6}	2.35×10^{-4}	3.24×10^{-5}	–	–	–
	2:1+meteo	–	–	1.41×10^{-6}	1.78×10^{-4}	2.99×10^{-5}	–	–	-7.7
	3:2+landcover	–	–	1.46×10^{-6}	2.50×10^{-4}	3.74×10^{-5}	–	–	15
	4:3+megan	–	–	2.62×10^{-6}	2.10×10^{-4}	3.31×10^{-5}	–	–	1.9
	5:4+emissions	–	–	2.35×10^{-6}	2.98×10^{-4}	4.54×10^{-5}	–	–	40
	6:5+physical	–	–	2.89×10^{-6}	2.44×10^{-4}	4.50×10^{-5}	–	–	39
$PM_{2.5}$ (μg.m^{-3})	1 :Base	0.47	6.25	3.71(0.17)	61.46(59.52)	11.13(4.88)	0.45	1.29	–
	2:1+meteo	0.39	6.29	4.49	36.26	11.17	0.40	1.27	0.3
	3:2+landcover	0.43	7.56	4.71	39.56	12.44	0.31	1.60	12
	4:3+megan	0.46	8.37	5.14	45.54	13.25	0.27	1.76	19
	5:4+emissions	0.47	8.54	5.33	48.10	13.42	0.30	1.76	21
	6:5+physical	0.47	6.07	4.28	39.84	10.95	0.45	1.25	-1.7
OA (μg.m^{-3})	1:Base	0.74	0.71	0.22(0.07)	13.80(20.35)	2.41(1.70)	0.54	0.39	–
	2:1+meteo	0.69	0.56	0.21	16.15	2.26	0.61	0.29	-6.3
	3:2+landcover	0.70	1.00	0.23	18.14	2.70	0.57	0.61	12
	4:3+megan	0.70	1.62	0.24	24.38	3.32	0.46	0.96	38
	5:4+emissions	0.70	1.73	0.25	25.22	3.43	0.44	1.01	42
	6:5+physical	0.70	0.99	0.22	17.68	2.69	0.57	0.59	11

4.1 Biogenic and anthropogenic primary gaseous species

The sum of monoterpenes is the first group of species that we consider here. Measurements of PTR-Tof-MS are compared to the simulated sum of α-pinene, β-pinene, limonene and ocimene concentrations. The m/z 137 peak as the main fragment of monoterpenes and m/z 81 values as their second most important one are taken for the PTR-Tof-MS measurements (refer to Li et al. (2020) and Li et al. (2021) for detailed information about treatment of PTR-ToF-MS measurements). Figure 6 shows a comparison of O_3 and terpene concentrations with measurements in different sensitivity tests, both shown in ppb (NO_2 is shown in the SI-5). It should be noted that each of these $BVOC$s have been compared separately to measurements as well; the comparisons are presented in the SI (Figures SI6 through SI11).

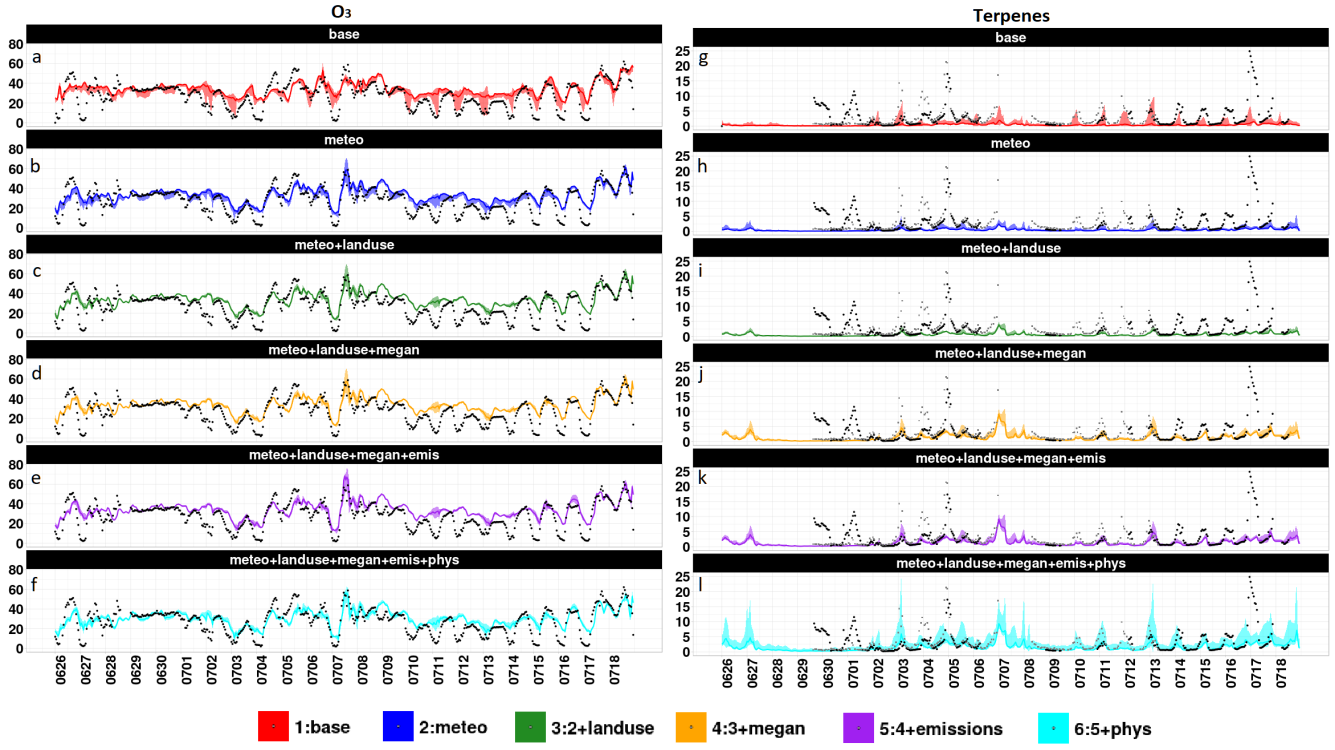

Figure 6. Time series for O_3 and terpene concentrations (all in ppb) for all the sensitivity cases explained above. The color schemes are shown on the right side. The name of each case is written above each time series. Time series for other species are provided in the supplementary information.

Terpene concentrations are source-dependent and being enhanced locally; they are more important near emission sources throughout the forest area (Figures 4 and 10). Observed and simulated terpene concentrations (Figure 6, panels g through l) show a marked diurnal cycle with increased night-time levels due to decreased sink processes (less OH and O_3, but more NO_3) and decreased horizontal and vertical dispersion (night-time wind speeds and exchange coefficients are minimal), as pointed out by Bsaibes et al. (2020) and Mermet et al. (2021). Observed night-time terpene maxima ranges between 5 and 25

ppb. Largest concentrations are reached during nights of July 2 – 3, 4 – 5, and 16 – 17. These peaks generally correspond to lower friction velocity observations (below 0.1 $m.s^{-1}$), and larger temperatures as pointed out by Bsaibes et al. (2020).

Simulated terpene maximum levels with the base case configuration barely exceed a few ppb, and can reach up to about ten ppb in the 11 km×11 km area around the Salles-Bilos measurement site. The night-time peaks during July 4 – 5 and 16 – 17 are not reproduced which may probably be explained by an overestimation of friction velocity during these nights (as seen in Figure 2, panel d). Increased day-time concentrations are simulated during the two hot weather periods (July 4 – 8, and July 16 – 18).

Some of the sensitivity cases explored in this study cause strong positive changes in the concentrations of terpenes: 11% when changing landcover inputs, +103% (always compared to the base case average) when updating biogenic emissions with local emission factors and +145% when changing the K_z parametrization. The 10% increase while changing the landcover is related to the tree density changes in the region; although it is interesting to keep in mind that changing the landcover may also decrease the tree density in the forest since some parcels were recently turned into agricultural fields. For the measurement cell, tree density increases by around 29%. The increase of terpenes when updating the biogenic emissions occurs because both the tree types and the tree emissions rates for the forest have been rectified in the emissions produced by the MEGAN model. Coherently, this also leads to a decrease (-73%) of isoprene concentrations, since changing the majority of the Landes forest tree type in MEGAN to maritime pine means that the density of isoprene emitting trees reduces significantly. Including the canopy parametrization in the model causes emitted terpenes to be less exchanged between inside the canopy and above. It also increases the variation of terpene concentrations locally, seen from the larger envelope around for the canopy effects sensitivity case in Figure 6. The other two test cases show slightly negative effects on the terpene concentrations (-10% and -2% for the meteorological test and the anthropogenic emission test case respectively). Figure 7 shows the distribution of isoprene/terpene in base case (panel a) and the final (panel b) sensitivity cases for the measurement cell compared to the distribution of different monoterpene/sesqui-terpene species in measurements (panel c). It is important to notice that this distribution changes substantially between the base case and the final case, being much closer to the observed distribution after the biogenic emission/landcover modifications. An overestimation of isoprene is still seen in the final case.

Finally, and importantly, the different test cases lead to a clear improvement in average and maximum simulated sum of terpene concentrations (see figure 6, panels g through l). In particular, the negative biases are strongly reduced for maximum terpene concentrations, from 14.0 ppb to 22.4 ppb as compared to 25.2 ppb in observations. It is also important to keep in mind that in the canopy test case, the changes seen in the concentrations come almost entirely from the K_z modifications and not from the modification made to the shortwave radiation.

Next, simulations of NO_2 as a tracer of anthropogenic emissions are discussed (Figure shown in the SI). Observed NO_2 level is at its maximum mostly during the night and early morning hours, reaching peaks between 3 and 7 ppb (for nights between July 2 – 3, 3 – 4, 6 – 7, 15 – 16, 16 – 17). Again, this is due to reduced local dispersion, in addition to suppressed NO_2 photolysis, and in spite of lower night-time NO_x emissions. Its NO_2 changes most in two cases: the anthropogenic emissions test case (+26%) and the meteorological test case (+20%). The refined distribution of anthropogenic emissions explains the major part of the first case, as average emissions over the inner model domain increase by only 4%. For the meteorological test

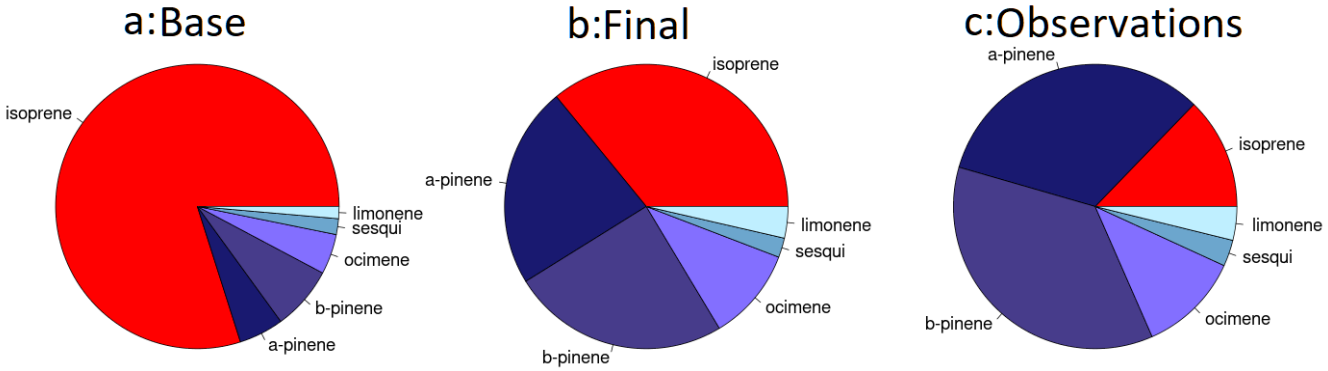

Figure 7. Pie charts of the distribution of $BVOC$s in observations, the base case and the final case scenarios. In the species presented here, every species represents only the species named apart from ocimene. Ocimene is the sum of mercyne and ocimene in the model, the same sum is presented for the measurements.

case, the changes to the maximum values of NO_2 are attributed to the advection of air masses from the Bordeaux metropole (or the main highway crossing the south west of France) towards the measurement site. For other scenarios, changes are all below 10%.

On the whole, average NO_2 concentrations of the model configuration specifically for the Landes forest are in better agreement with observations compared to the standard version (-0.69 instead of -0.99 ppb for the bias (simulation - observation) and 0.62 instead of 0.43 for correlation coefficient compared to observations (refer to Table 2). Please note, that due to the non-specificity of NO_2 measurements, they could overestimate actual concentrations. On a relative scale, this is expected to be less important for peak values indicating the presence of fresh NO_x, than for unpolluted periods when the NO_x/NO_y ratio may be low.

4.2 Secondary gaseous species: ozone

Changes of sensitivity tests for O_3 will be discussed here. O_3 can be considered a representative of gaseous secondary species, as well as governing the oxidation of $BVOC$ species directly or indirectly leading to $BSOA$ formation. O_3 concentration values show a strong diurnal variation due to photochemical formation during day-time and dry deposition and depletion by terpenes during night-time. Largest day-time O_3 maxima levels during the campaign were between 55 – 60 ppb during the so called "strong oxidation" periods characterized by elevated temperatures, low relative humidity, and low wind speeds (< 3 $m.s^{-1}$) from July the 4^{th} to the 7^{th} then from the 14^{th} to the 18^{th}. The higher values of O_3 are due to continental advection under easterly wind conditions (visible when looking at the continental domain simulations). Lowest night-time concentrations were observed for nights between July 2 – 4, 6 – 7, 14 – 17), corresponding to reduced local dispersion and enhanced NO_2 concentrations. In the early morning hours of such nights, observed in-canopy O_3 levels could even drop close to zero, due to depletion by mainly terpenes, dry deposition, and suppressed vertical mixing. While simulations with the standard model

version correctly reproduce the day-time O_3 maxima, they significantly overestimate the O_3 minima; simulations never show below 20 ppb while measurement minima can reach 0 during nighttime.

Daily O_3 maxima are only slightly changed in sensitivity tests, the largest impact being noted for the test with refined emissions, leading to enhanced NO_x emissions and an increase in the O_3 peak on July 7 from about 60 to about 70 ppb (Figure 6 and Table 2). It should be mentioned that while the maximum change in maxima of O_3 is seen in the emissions test case, the maximum for the aforementioned day already changes when the meteorological inputs are modified in test case 2. The increase in terpene emissions does not lead to an increase in O_3 production, partly because it is compensated by a decrease in isoprene.

Night-time O_3 minima tend to decrease in different sensitivity tests. Here it is interesting to check if the simulations can reproduce the lowest night-time values obtained between July 2 – 4, 6 – 7, 14 – 17. Alternative meteorology from ECMWF instead of NCEP/WRF leads to lower friction velocities during these nights and thus lower O_3 minima, from 19.2 ppb to 14.8 ppb for the average over these nights. Landcover and emission factor changes do not affect O_3 minima to a significant degree (only 0.8 ppb of decrease for both cases), probably because terpene increases are compensated by isoprene decreases, resulting in rather unchanged O_3 depletion. Emission changes affect these minima slightly (1.5 ppb of decrease for the minima when emissions are changed), probably because of increased titration with NO leading also to increased night-time NO_2. Including the canopy parametrization leads to a decrease in O_3 minima (inside the canopy), due to decreased vertical exchange and less O_3 transfer from above (from 12.9 ppb to 10.4 ppb).

However, even the refined model configuration still overestimates O_3 nightly minima (10.4 ppb instead of 2.0 ppb observed for the three periods of July 2 – 4, 6 – 7, 14 – 17) even if this overestimation has decreased with respect to base case (19.2 ppb instead of 2.0 observed). Also, the lowest simulated O_3 concentrations in the 11 km$\times$11 km domain around Salles-Bilos site, are still above the observed ones. This is not without consequences for oxidant supply for night-time SOA build-up from terpenes, which is then overestimated for these nights. Reasons for this O_3 overestimation are unclear. Titration by terpenes and NO seem to be correctly taken into account as night-time peaks of these compounds seem well-simulated (see section 4.1 above for comparison to measurements, Figure SI-5 for NO_2 and Figure 6 and Table 2). It can be because of missing sources for minor terpenoids, which even in low concentrations can be extremely reactive in the atmosphere making them capable of consuming practically the entirety of night-time O_3. Another plausible candidate for this issue could be an underestimation of deposition of O_3 over forested zones. However, the dry deposition velocity of this species was compared to calculated dry deposition velocity using measured O_3 fluxes. This speed is well simulated with an average of 0.43 $m.s^{-1}$ and 0.62 $m.s^{-1}$ for observations and simulation respectively (Figure shown in SI-3).

Therefore, an additional unrealistic sensitivity test was performed, putting vertical exchange coefficients to zero during night-time (between 22h and 5h every night only for grid cells with tree density higher than 70%). This leads to closer O_3 night-time values compared to measurements (1.9 ppb), but to unrealistically high terpene concentrations (concentrations of over 50ppb). Still an overestimation of canopy to outside exchange could be a reason for not displaying the near zero O_3 values.

4.3 Radical species

Radicals (shown in Figure 8) play a major role in atmospheric chemistry. NO_3 has been recognized as a major oxidant especially of terpenes (for example see Ng et al. (2017)). The NO_3 IBBCEAS measurements available for this campaign were always below the detection limit of 3 – 5 ppt (M. Cirtog, personal communication). In the base simulation and the meteorological and the landcover test cases, night-time maxima can reach 1 – 3 ppt. When the concentration of terpenes is increased (i.e. in the biogenic emissions test case), night-time NO_3 concentration maxima are limited to below 0.5 ppt with one exception. The canopy parametrization leads to additional NO_3 decrease, because of increased terpene concentrations (and probably minor effects due to the NO_2+O_3 source reaction flux). The night-time overestimation of O_3 minima probably leads to an overestimation in NO_3 concentrations. Interestingly, Mermet et al. (2021) calculated the NO_3 concentrations through steady state equations inside the canopy using measured NO, NO_2, O_3, monoterpene and isoprene concentrations as well as radiation parameters. They found day-time maxima of up to 0.1 ppt in contrast to our simulated night-time maxima (the reason for the calculation of a daytime maxima by the aforementioned study for a species that should not have significant day-time concentrations is unclear). These changes and differences potentially affect SOA formation, as will be discussed in the next section.

Compared to NO_3, OH concentrations remain more stable among in all sensitivity cases, changes being generally limited to several tenths of %. These changes are difficult to explain in absence of a dedicated budget study which is beyond the scope of this paper. For instance, the combined effect of landcover and $BVOC$ emission changes is relatively small, probably because of increased loss reactions with terpenes are compensated by diminished loss with isoprene. Increases in daily maximum OH due to anthropogenic emission changes could be due to a more effective OH recycling via the NO + HO_2 reaction. When it comes to the canopy test case, the modification of swrd results in a decrease in OH concentration by a factor of 1.4 on average, while the K_z and wind speed modification does not result in any significant change on the concentration of OH. For more densely forested grid cells, the in-canopy radiation has a higher reduction and as a consequence so does the OH concentration. Since no OH concentration measurements were available from this campaign (the FAGE instrument deployed by the University of Lille having unfortunately encountered technical problems), they have been estimated from in canopy global radiation, and a climatological (above canopy) maximum OH concentration $3-6\ 10^6\ molecules.cm^{-3}$ (Mermet et al., 2021). Daily OH maxima estimated in this way were about a factor of 2 to 3 below our simulated in-canopy concentrations.

4.4 Particulate species

Figure 9 shows the comparison of all performed sensitivity cases to measurements at the Salles-Bilos site for particulate species, all values being in $\mu g.m^{-3}$. $PM_{2.5}$ observations during the campaign period culminate at more than 20 $\mu g.m^{-3}$ on July 7^{th}. Some higher hourly values (also visible in OA) on July 6^{th} are due to a local fire which is not further analyzed here. About half of $PM_{2.5}$ is composed of organic aerosol (10 $\mu g.m^{-3}$). The simulated concentrations of secondary inorganic aerosol (sulfate + nitrate + ammonium), sea salt, black carbon and dust are about 3.0, 1.6, 0.9 and 7.6 $\mu g.m^{-3}$ respectively in the model, pointing to a significant dust contribution at this time at Salles-Bilos. The base case simulations show large $PM_{2.5}$

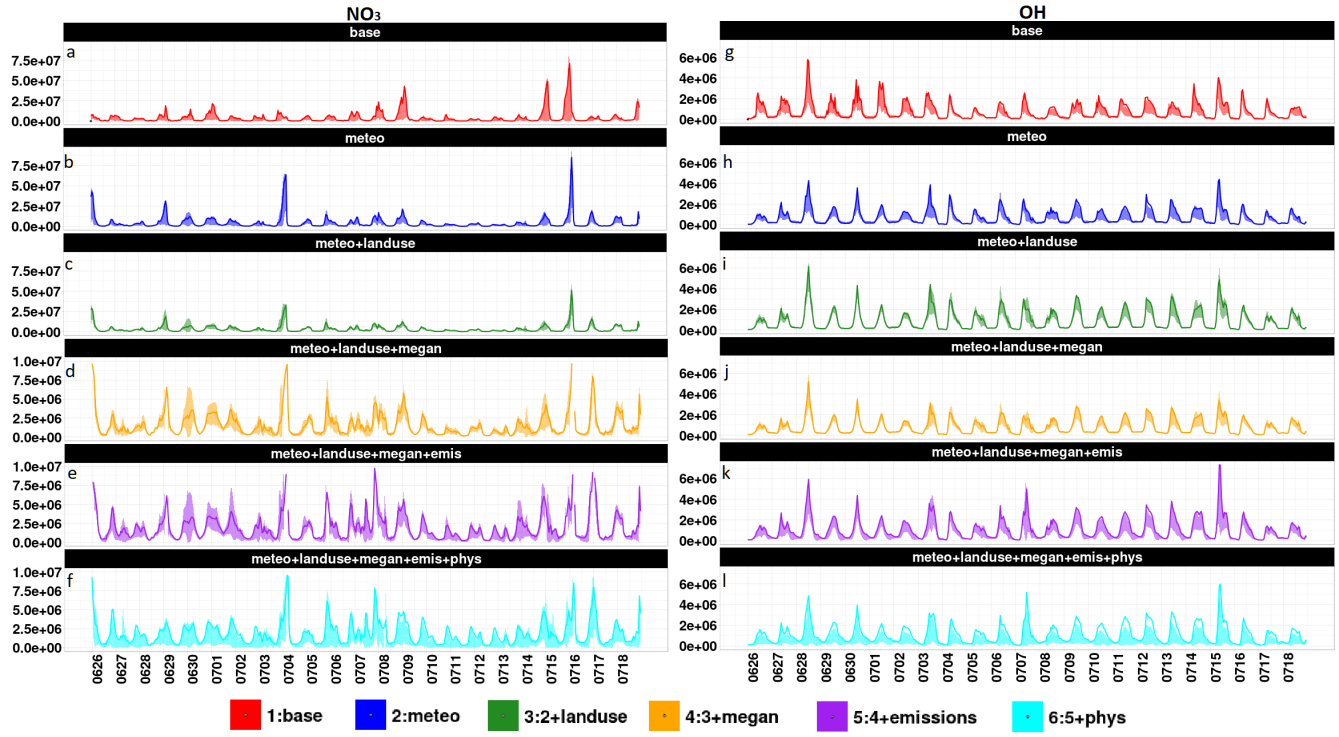

Figure 8. Time series for OH and NO_3 concentrations (both in ppb) for all the sensitivity cases explained above. The color schemes are shown on the right side. The name of each case is written above each time series. Note that the NO_3 columns have 2 different scales because of visibility issues. Both plots are in $molec.cm^{-3}.s^{-1}$, the scale for NO_3 changes for certain test cases.

concentrations around this date (from July 6^{th} to 9^{th}) at Salles-Bilos, reaching 60 $\mu g.m^{-3}$. This species is very sensitive to the chosen meteorology; with ECMWF meteorology, the peaks decrease to 40 $\mu g.m^{-3}$, however another dust related, yet unobserved peak at Salles-Bilos occurs on July 13^{th}. Both of these episodes were seen in AOD observations at the Arcachon AERONET station (a city to the west of Bordeaux, near the coast line).

Besides dust, OA is the main driver of observed and simulated $PM_{2.5}$ variability. During the sunny, calm and high oxidation periods, from July the 4^{th} to the 7^{th} then from the 14^{th} to the 18^{th} observed OA concentrations reach about 10 $\mu g.m^{-3}$. This time pattern is rather well reproduced by the base simulation, OA peaks are however overestimated (see below). It is concluded from the model results and known OA sources, that most of it is biogenic SOA (84% in simulations at Salles-Bilos over the campaign period). For instance, the concentration of anthropogenic OA (primary and secondary is quite low at this site (average of 0.11 $\mu g.m^{-3}$ over all test cases).

Average OA concentrations (Figure 9) are mostly impacted by the biogenic emissions sensitivity case (+26%), the canopy test case (-24%), the landcover changes (+22%) and the meteorological test case (-7%). The test case that has the least effect on the concentration of OA is the anthropogenic emission test by a +3% increase. Changing the biogenic emissions causes a significant increase in the concentrations of terpenoids (sum of mono and sesqui-terpenes), which then increases the for-

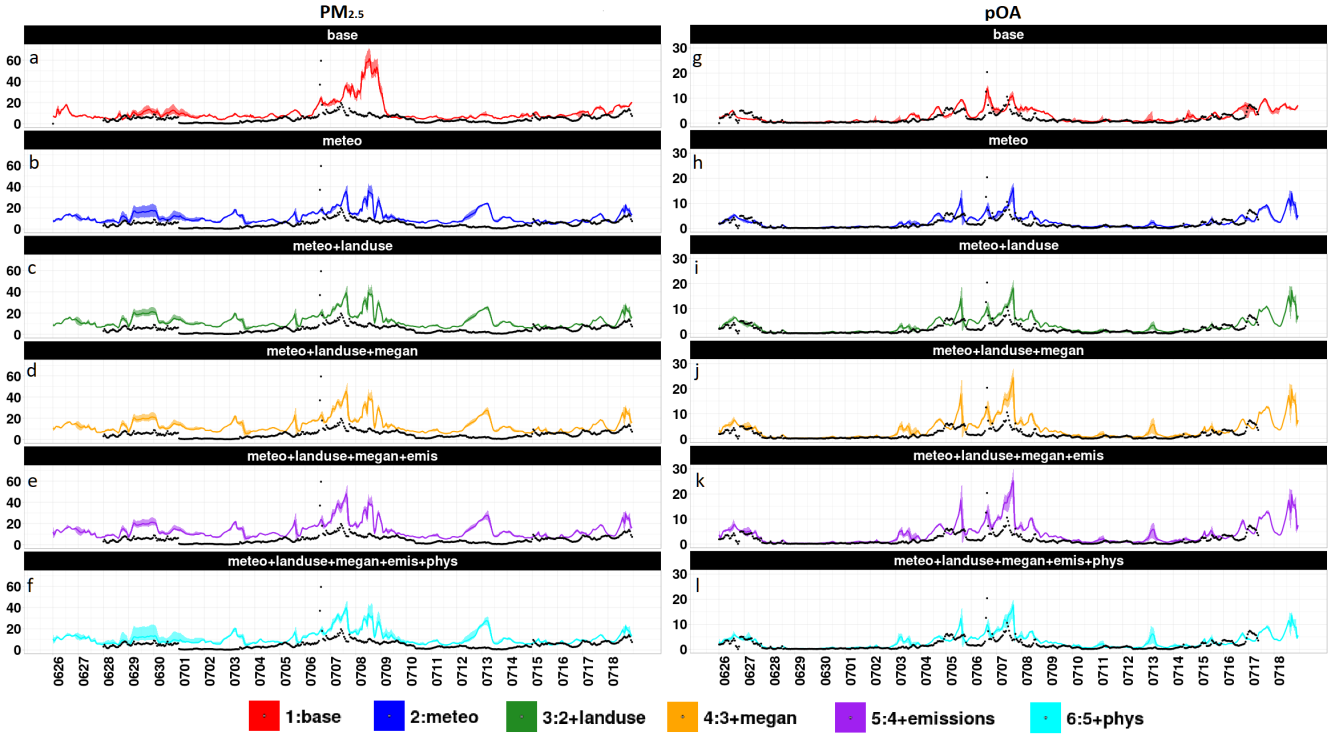

Figure 9. Time series for $PM_{2.5}$ and organic aerosols (OA) both in $\mu g.m^{-3}$ for all the sensitivity cases explained above. The color schemes are shown on the right side. The name of each case is written above each time series.

mation of biogenic OA. The landcover changes also impact the concentration of OA for the same reason. Changing the K_z parametrization and in canopy radiation decreases both OA and $BSOA$, as well as the concentrations of the three oxidants (OH, NO_3 and O_3) which participate in the biogenic OA formation process, while increasing the concentrations of terpenes (its major precursors). So, a lesser portion of the emitted terpene is oxidized and less BSOA is therefore formed.

The final test case shows enhanced OA concentrations with respect to the base case, an additional difference lies in the chemistry behind the production of OA as it will be discussed in section 4.5; in the final test case the concentrations of precursors and radicals correspond better to observed data, as shown in the previous sections. The remaining overestimation can be due to the already stated oxidant overestimation for O_3 and NO_3 (noting that OH cannot be verified). It can also be due to the scheme used for the simulation of OA; thus, forthcoming work should test the sensitivity due to different aerosol scheme.

4.5 $BSOA$ formation from different precursors and oxidant pathways

As pointed out in the introduction, different precursor/oxidant pathways for $BSOA$ build-up have been found in the literature (e.g. Hallquist et al. (2009), Xu et al. (2015), Qin et al. (2018)) for different types of forest, and it is interesting to address this

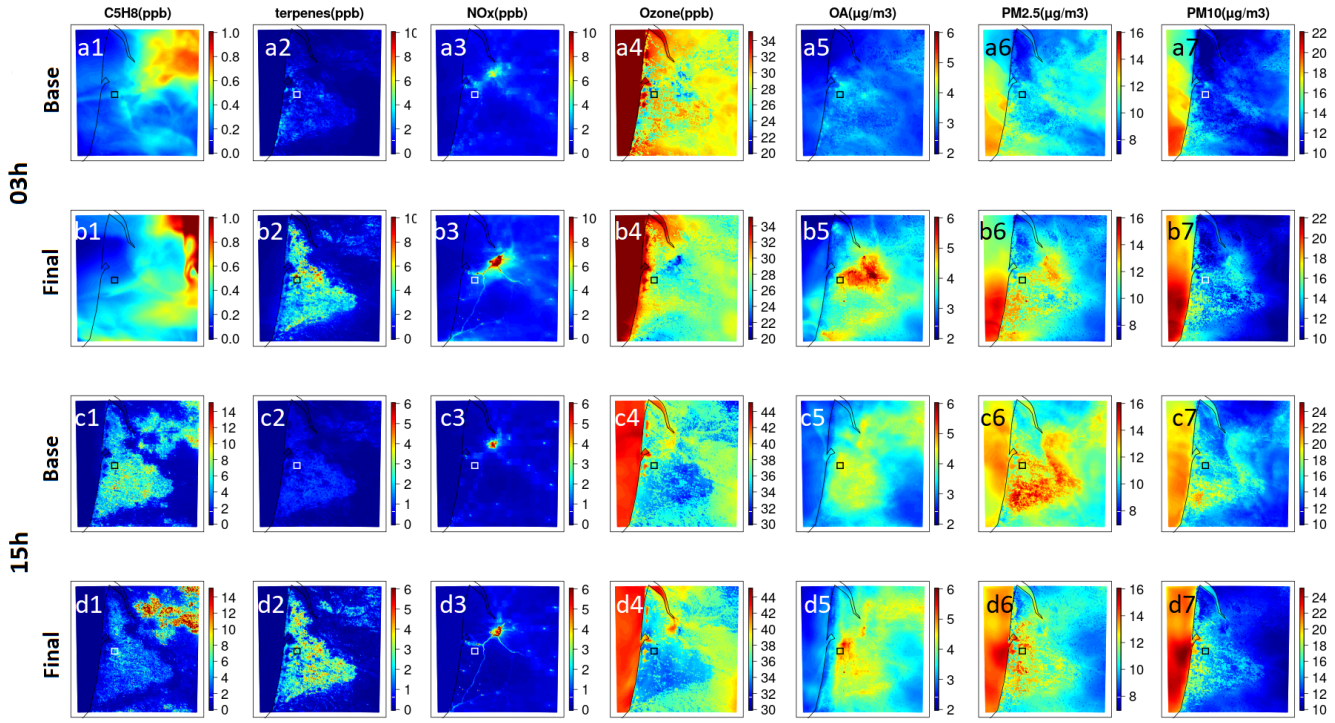

Figure 10. 2D figures showing average concentrations over the campaign period for species of importance for this study (compound names and associated units written above each column) for 3h (first two rows) and 15h (second two rows) for base (first and third rows) and final simulation (second and forth rows). Note that the scales are different for each figure. The measurement site at Salles-Bilos is located in the middle of the white or black rectangle of 10km x 10 km extension.

question for a maritime pine forest. To do so, two sets of additional simulations have been performed for the base case and the final case, in which the formation of BSOA from each precursor and via each oxidant was followed individually during the model run. These results are presented in Figures 11 and 12.

For the base case scenario, the formation of $BSOA$ is achieved in majority from isoprene oxidation by OH. After the corrections made for the landcover, the tree types and the physical parameters (introduced in section 3.6) in the final test case, isoprene + OH stays the most important $BSOA$ formation pathway, but monoterpenes become the dominant precursor group. The attack of β-pinene by NO_3 is noteworthy in this group, in accordance for example with results found for the 2013 SOAS study in South-Eastern US (Xu et al., 2015). The reaction of sesqui-terpenes with O_3 is a third important reaction pathway.

Looking at which oxidant is responsible for $BSOA$ formation, the majority of $BSOA$ in the base test case is formed from OH radical reactions (by about nearly the half, i.e. 47%), followed by O_3 (nearly 30%) and NO_3 (more than 20%). In the final test case, the $BSOA$ formation becomes more evenly distributed between the three precursors: OH, staying in majority (by 36%) while the other two oxidants follow closely (33% for NO_3 and 31% for O_3). These results can be compared to those reported by the $BVOC$ reactivity study at Salles-Bilos (Mermet et al., 2021), based on measured $BVOC$ species and O_3,

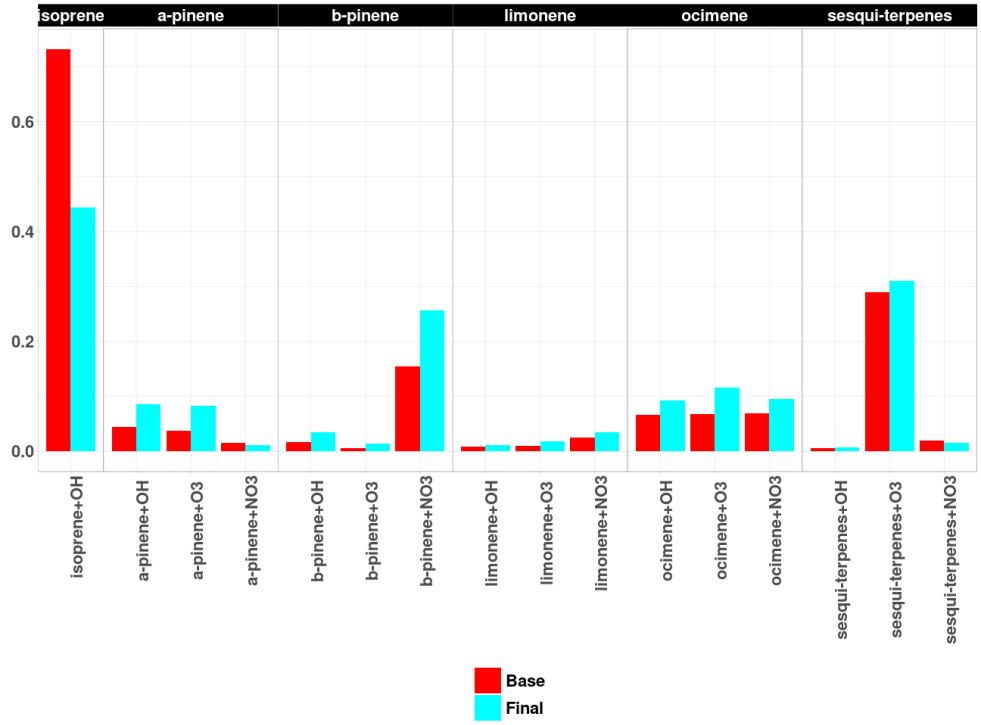

Figure 11. Barplots showing the campaign period averaged formation of $BSOA$ (in $\mu g.m^{-3}$) from all precursors and oxidants. Name of the simulation is written below the barplots. The reactions are shown on the x axis.

and OH and NO_3 estimated from chemical equilibrium and solar radiation, even if this work addresses different features. In this study, the β-caryophyllene + O_3 reaction makes by far the largest contribution to $BVOC$ reactivity. In our simulations, β-caryophyllene is part of the sesqui-terpene species family, which still makes an important contribution. Also, monoterpenes strongly contribute to $BVOC$ reactivity, while isoprene is only a minor contributor. In general, O_3 is the major oxidant, followed by OH, while NO_3 only makes little contributions. Differences with respect to the experimental study (Mermet et al., 2021) to our study can be explained by many factors which we do not attempt to quantify here: (i) the experimental study considers local oxidation rates, and those within the canopy are used here, while our study considers contributions within air masses arriving at the receptor site; (ii) our study overestimates night-time O_3 which leads to high NO_3 radical formation (see Figure 8), and could explain the larger share of NO_3 oxidation pathways; (iii) in the experimental study estimated OH is smaller than that in our study (see section 4.3); (iv) the initial share of $BVOC$ species might be different even if Figure 7 shows a broad agreement for major $BVOC$ species in the final case.

Interesting insight can also be obtained from analyzing the daily averaged concentrations of BSOA being formed from the different reaction pathways of BVOCs with oxidants presented in Figures 11 and 12. While the concentration of total $BSOA$ stays quite similar between the two simulations (with the exception of some days and especially July 7^{th}) the chemistry behind

their formation changes significantly. The contribution of isoprene in the formation of $BSOA$ becomes lower in the final case, while the contribution of the β-pinene + NO_3 pathway, and of the oxidation of other terpenes increases significantly. Figure 12 shows that this is especially true for 07^{th} of July when simulated BSOA was most overestimated. As terpene levels were well simulated on this day, this could most probably be due to an overestimation of radical concentrations (NO_3 and OH) and/or SOA yields. However, as many different pathways contribute to $BSOA$, it is difficult to pinpoint a specific one as the responsible for this $BSOA$ overestimation.

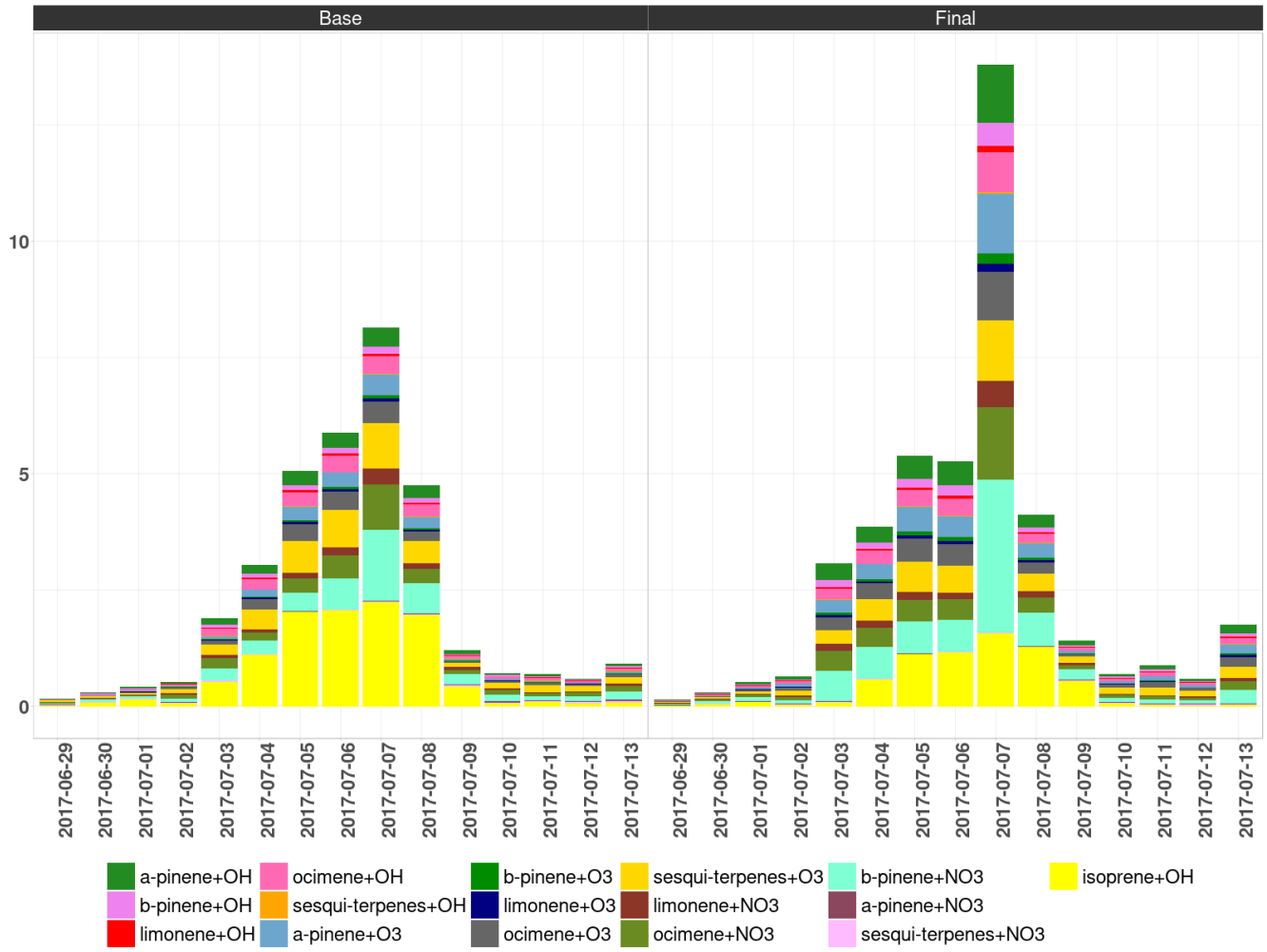

Figure 12. Daily averaged concentrations of $BSOA$ per precursor and per oxidant in $\mu g.m^{-3}$. The colors per each reaction are given under the figure. Base case simulation results are shown on the left, while the final case results are shown on the right.

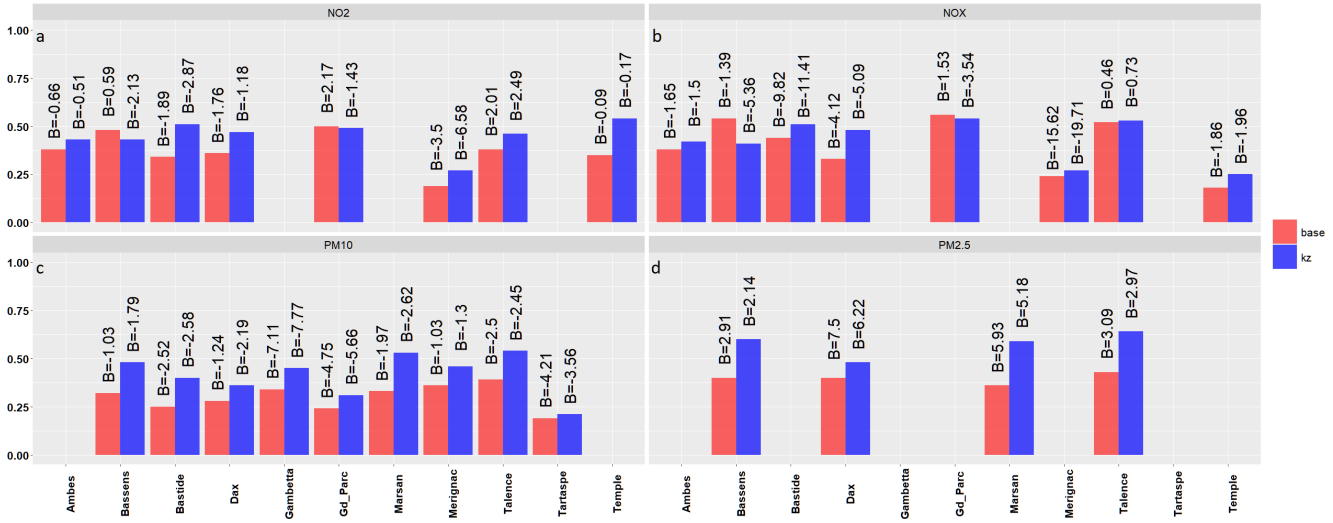

Figure 13. Statistics for the comparisons of measurements performed in air quality stations for NO_2, NO_x, PM_{10} and $PM_{2.5}$ and the simulations. The y axis shows the correlation coefficient while the bias (simulation - observation) for each station is written on each bar. The comparisons involve the base case (in red) simulation and the final test case (in blue).

5 Spatial distribution of $BSOA$, precursors and oxidants over the Landes forest

5.1 Average spatial distribution during the Landex campaign

After this first analysis of time series at the measurement site where intensive campaign data was available, we now would like to extent the discussion to a broader spatial scale, covering the Landes forest and its surroundings. To achieve this, we first present near surface 2D maps (of the high-resolution domain covering the Landes forest) of specific species pertaining to our study averaged over the campaign period (between 26^{th} of June to the 20^{th} of July 2017). The interest here is to analyze, how the changes in the model from the baseline test case to an updated local/regional configuration modifies the concentrations seen in these 2D fields.

Due to the short lifetime of terpenes during day-time (a few hours in most cases), the area of enhanced total terpene concentrations (at 15h UTC) closely corresponds to the high emission zone of the Landes forest. In the high-resolution simulation (1 km) with the canopy parametrization and all other local databases, average terpene concentrations are heterogeneous; varying from some ppb to up to 10 ppb. During night (3h UTC), terpene levels are maximum near the north east edge of the forest. This is due to larger emissions there (Figure 4, panel c), but also to lower O_3 concentrations leading to diminished loss (Figure 10). The higher concentration of O_3 observed over the ocean in Figure 10 (panels a4 to d4) is because of the lower deposition of O_3 over bodies of water, since its dry deposition speed is lower.

As expected, a strong increase is seen in the final case compared to the base case test over the whole domain. This is mainly due to enhanced terpene emissions in the local databases.

Isoprene concentrations in the final case simulation are also enhanced over the Landes forest; they are higher over forested areas in the north east of Bordeaux, which include more isoprene emitting species like oaks.

The NO_x 2D fields display largest concentration levels in the urban Bordeaux area, even larger at night due to enhanced vertical stability. In the simulation using a high resolution emission inventory, highways starting from Bordeaux are displayed, such as weak plumes in the surroundings of the city. It is also interesting to compare the difference in resolution in base and final simulations, noticeable in the 2D images shown in Figure 10 (panels a3 to d3). Daytime NO_x concentrations in the Landes forest are relatively low (typically 2-3 ppb). According to this, photochemical O_3 production is not very active over the Landes forest, since day-time O_3 levels are lower there (35 – 45 ppb) than in surrounding areas (45 – 55 ppb), mainly due to loss by reactions with terpenes or by dry deposition, with exception of an O_3 plume in the SW of Bordeaux. Night-time O_3 shows local minima in the surroundings of the metropole, below 20 ppb, due to NO titration. If the results seen in Salles-Bilos can be extrapolated to the whole Landes forest, then simulated night-time O_3 levels are likely to be overestimated. Maximum values of NO_x do not change between base case and final simulation; however, their spatial precision improves because of the increase in the resolution of emissions inventory in the emission test case onwards.

Night-time OA in the updated configuration shows a hot spot at the north east edge of the Landes forest, corresponding to regions with enhanced terpene concentration levels. This effect is not seen in the baseline simulations, where concentrations are higher in the center of the forest (Figure 10). The night-time concentrations for the base case simulations are also lower. Day time OA is generally enhanced over the Landes forest, showing that large terpene emissions there lead to local OA build-up. In this averaged field, no $BSOA$ export from the Landes forest can be distinguished. Maximal concentrations occur within the forest at about 25 km from the coastline. It is hypothesized, that they are related to a sea breeze front forming along the Atlantic shoreline. This is also suggested by the 15h UTC temperature fields (not shown) which show large gradients (nearly 10K) between the coast and about 20 km inland. This phenomenon will be addressed in more detail in the next section. This sea breeze is also seen in the baseline simulations, when looking at hour-by-hour changes in OA concentration. In the base case simulations concentrations are lower in day-time as well, similarly as what was seen at night-time.

It can be noted that simulated $BSOA$ concentrations alone are above the WHO target of 5 $\mu g.m^{-3}$ for $PM_{2.5}$, even if they are expected to be lower during other seasons (however, we had shown above that they are overestimated with respect to measurements at the Salles-Bilos site). The spatial structure of $PM_{2.5}$ and PM_{10} simulations follows broadly that of $BSOA$ simulations with a major exception over the sea, where sea-salt makes an additional contribution to PM_{10}.

The concentrations of the base sensitivity test and the final sensitivity case were compared to regional air quality station measurements discussed in section 2 (Figure 13). These comparisons (panel a) show that the bias (simulation - observation) for NO_2 for all stations (regardless of the type of station) for the final test drops to -1.4 ppb (from an initial -2.9 ppb for the base simulation), while the averaged correlation coefficient gets to 0.42 in the final test from 0.37 for the base case. NO_x concentrations show a bias (simulation - observation) and correlation coefficient of -2.4 ppb and 0.57 in the final test case compared to -3.1 ppb and 0.51 in the base simulation respectively (panel b). Unfortunately, the concentrations of O_3 (while being measured) in the air quality stations weren't available for comparison for the period of simulations.

Figure 13 (panels c and d) also illustrates the comparisons of $PM_{2.5}$ and PM_{10} at air quality stations of the ATMO-NA network. It is interesting to notice that the profile seen in all stations is quite similar to each other. For PM_{10}, the results show an average correlation coefficient of 0.3 and 0.42 and an average bias (simulation - observation) of -3.3 $\mu g.m^{-3}$ and -2.9 $\mu g.m^{-3}$ for PM_{10} for the base and the final sensitivity test respectively. For $PM_{2.5}$ and for the base and the final sensitivity test respectively, a correlation coefficient of 0.4 and 0.58 and a bias (simulation - observation) of +4.8 $\mu g.m^{-3}$ and +4.1 $\mu g.m^{-3}$ is seen. Apparently, refining the simulations through the sensitivity tests adds physical information, as can be seen by the improved correlation coefficients (for PM, but also for NO_x).

5.2 A case study for the impact of sea breeze fronts

In the previous section, mention was made of the crest of the high afternoon $BSOA$ levels within the Landes forest about 25 km from the coastline, with the proposed hypothesis of a potential sea breeze front forming along the Atlantic coastline. Indeed, Planchon and Cautenet (1997) note that sea breeze fronts can go up to 40 km into the continent at the french Atlantic coast, other references show similar values (i.e. Lerczak et al. (2001)) while Hughes and Veron (2018) show a maximum of 200 km inland movement in specific situations. In this section, we wish to address this feature by a case study during the low wind period from July 5^{th} to 7^{th}, which should be prone to the development of sea breeze systems. Figure 14 shows the time evolution of $BSOA$ (panels a1 to a6 for the 5^{th} and panels d1 to d5 for the 7^{th}) during both July 5^{th} and 7^{th} (a path to an animation is accessible in the SI-7). It shows a tendency of $BSOA$ being transported to the coast by easterly winds during night-time (shown only in animations). Then they show the development of a sea breeze front approximately starting at noon, and progressing into the land during the afternoon. This front is materialized by pronounced gradients in temperature (warmer on the land side, panels b1 to b6 and e1 to e5), and the ridge in high $BSOA$ in vicinity of the front. Wind fields well depict this sea breeze system (panels c1 to c6 and f1 to f6). These figures dramatically show that in addition to chemical $BSOA$ formation, visible for example by comparing pictures for July 5^{th} 11h UTC and 14h UTC, such transport processes are major drivers for the $BSOA$ variability over the Landes forest.

This phenomenon is also affecting the species time series at the Salles-Bilos site and needs to be taken into account to interpret the Landex campaign data, in addition to the general synoptic situation and local dispersion conditions on which previous studies have already focused on (Kammer et al. (2018), Bsaibes et al. (2020), Mermet et al. (2021)). Figure 15 shows the passage of the sea breeze front at Salles-Bilos, as a concomitant sharp decrease in $BSOA$ and temperature during afternoon hours. Differences in the exact timing of the frontal passages are visible especially for July 7^{th}, when observed organic aerosol concentration at the Salles-Bilos site drops earlier than the simulated one. This could be due to other factors as for example an increase in boundary layer height not accounted for in the simulations.

6 Conclusions

This work aims to study the formation of $BSOA$ in a forest canopy using the CHIMERE chemistry-transport model. For this purpose, we have examined the Landes forest, one of the largest pine forests in Europe located in south-wester of France.

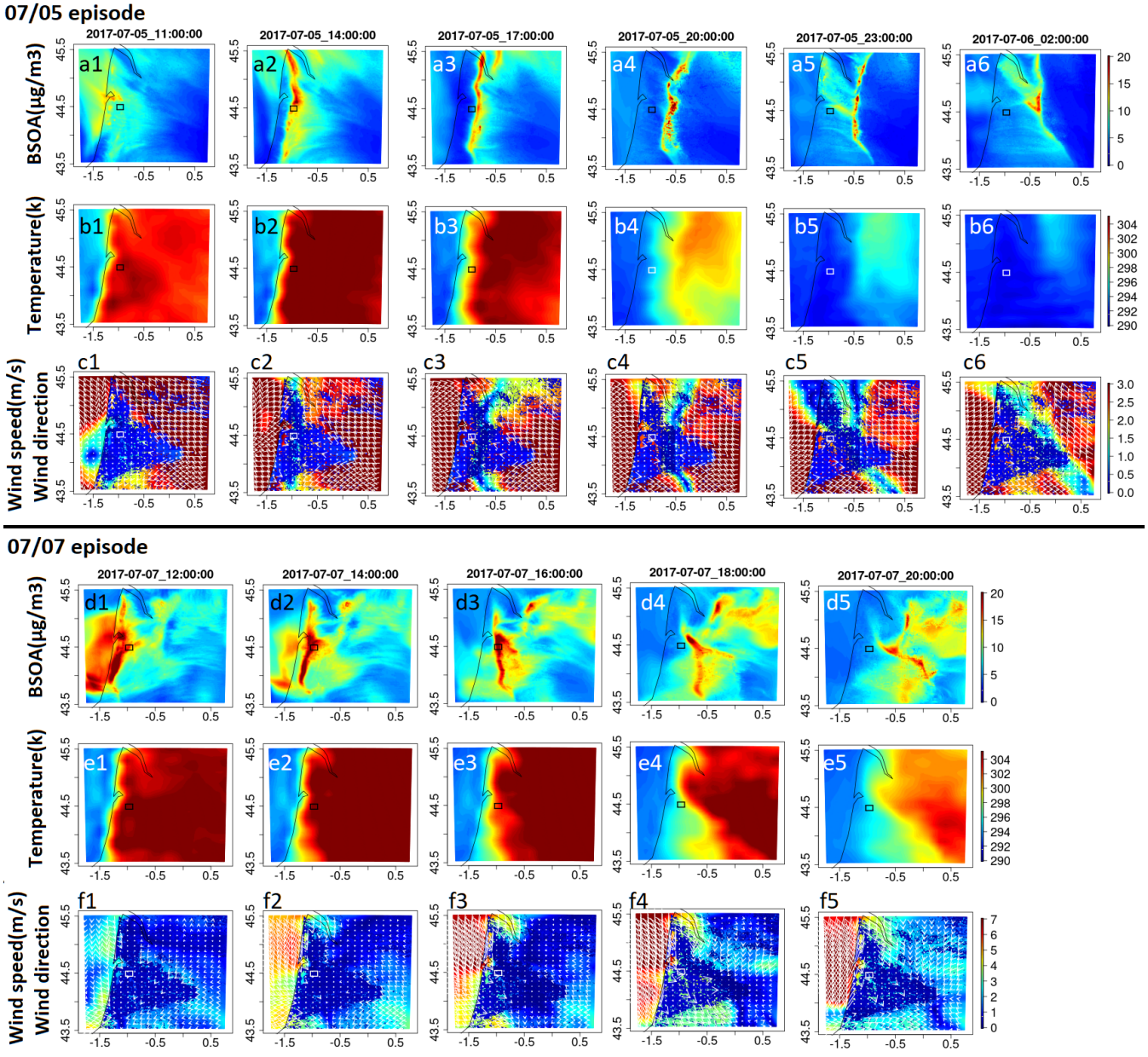

Figure 14. Sea breeze event for the 5^{th} and 7^{th} of july. The date and time for each pannel is shown on the top of each panel, each row represents one variable/species, the name and the unity mentioned on the side.

The forest is populated by a 95% majority of maritime pines, a mono and sesqui-terpene emitting tree species. It is also a region with rather homogeneous landcover, and weak anthropogenic influences. The measurements used in this study were performed during the LANDEX episode 1 field campaign, carried out in the summer of 2017 with the goal of understanding

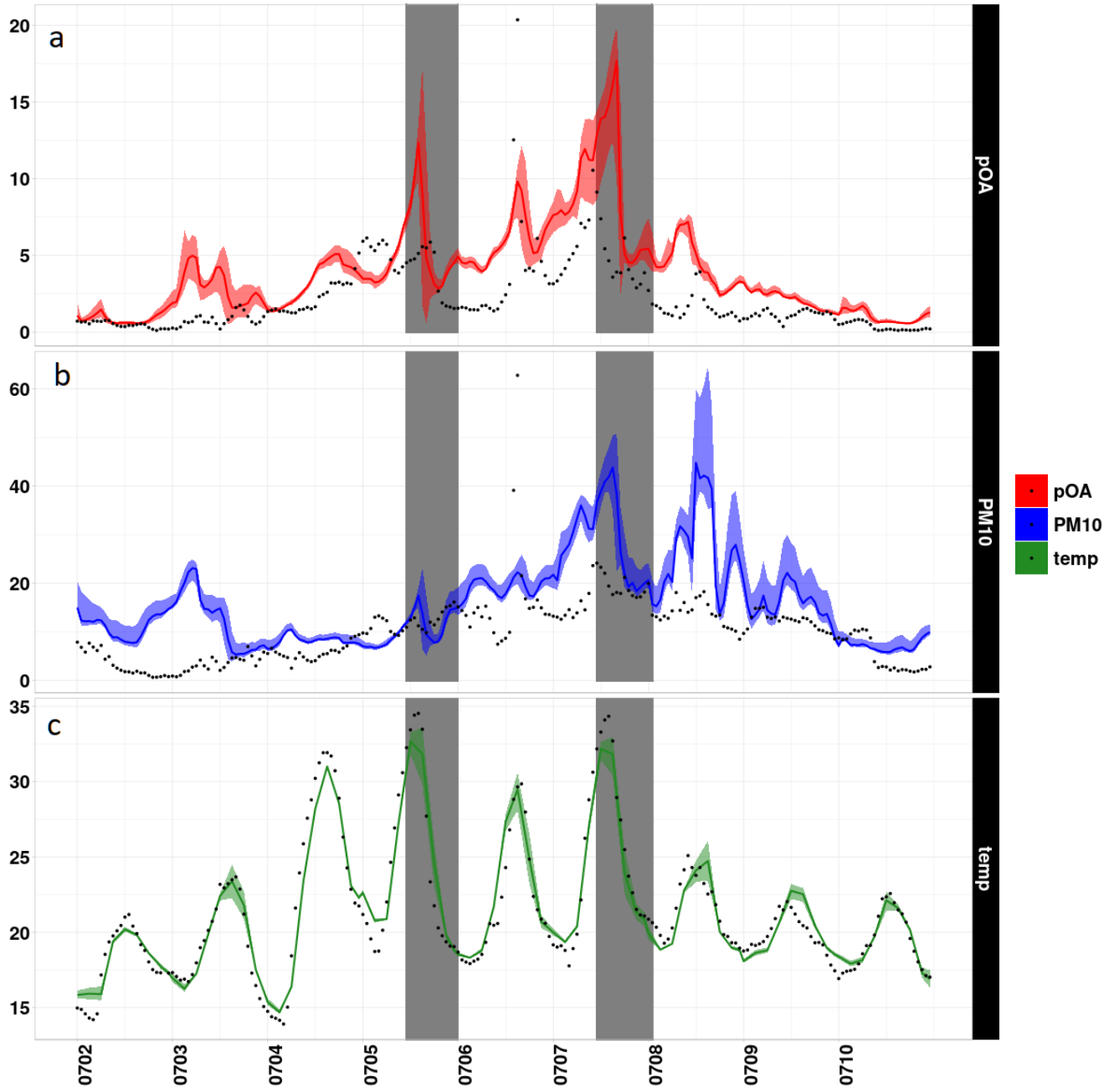

Figure 15. Time series for $BSOA$ ($\mu g.m^{-3}$), PM10 ($\mu g.m^{-3}$) and temperature (k) for the two sea breeze episodes compared to measurements. The episodes are highlighted on each panel. The confidence interval corresponds to the concentrations seen in a 11kmx11km square around the measurement site. The grey zones correspondent to times of passage of the sea breeze front.

the atmospheric chemistry related to biosphere-atmosphere interactions. At the Salles-Bilos site within the Landes forest, a set of detailed in-situ measurements has been obtained to illustrate these features.

In order to study the formation of $BSOA$ we had to first focus on the entire physico-chemical system inside the forest canopy. Therefore, we performed multiple test cases updating the representation of the forest in the chemistry-transport model. It has to be kept in mind that while the goal is partially improving the performance of the model for this specific region, the sensitivity cases are also meant to show the effects of changing inputs or the simulation of different physical parameters on the concentration of different atmospheric species. Since the CHIMERE chemistry-transport model does not include an on-line canopy model, we have tried to mimic the simulation of a forest canopy by adding region-specific parametrizations.

The modelling chain consists of three nested domains, one covering the entire Europe, the intermediate one focused on France and the last nested domain focused entirely on the Landes Forest with a horizontal resolution of 1 km. In total, 6 sensitivity cases were performed, focusing on meteorological input fields, landcover inputs, improving the biogenic emission factors by correcting the type of trees present for this region in the MEGAN model, anthropogenic emissions and finally adding a parametrization prepared specifically for the Landes forest for the simulation of vertical diffusivity, wind speed and penetration of radiation inside the forest canopy.

Each of the studied scenarios shows effects on different species, for example not surprisingly NO_x are quite sensitive to changes in anthropogenic emission inputs, while terpenes show a double sensitivity to changing the emission factors as well as changing the vertical diffusivity and wind speed in the area. What has been noted as the physical test case (taking into account physical changes to the simulations of vertical diffusivity, wind speed and radiation penetration inside the canopy) presents a closer representation of the measurements observed in the Salles-Bilos site as well as of several air quality measurement stations around the forest. Using the final and the base test cases, we also simulated the formation of $BSOA$ from different precursors and oxidants. This showed us that the formation of $BSOA$ for the base case scenario comes from the wrong precursors, as $BSOA$ is mostly formed from the oxidation of isoprene which is not accurate for this region. The formation of BSOA changes to terpenes (specifically sesquiterpenes and β-pinene) in the final simulations, which is more in line with the observations in the Landes forest. These final results are more in line with what is seen in the measurements for the Landes forest as well.

We also make evident spatial gradients between the forest and the surrounding areas especially for $BSOA$ and short-lived species like terpenoids and isoprene. The formation of $BSOA$ is quite localized inside the forest, consistent with high $BVOC$ reactivity (which leads to $BSOA$ formation in one step in our model, so in reality BSOA formation could take some more time as a multi-step process). We also evaluated our simulations at regional scale which showed an improvement in almost all stations for all species measured at air quality stations located around the forested area. Still, for $PM_{2.5}$ a positive bias (simulation - observation) subsides, probably caused by the positive bias in OA, a major contributor to $PM_{2.5}$ concentration.

In addition, we analyzed the impact of transport processes within the forest area, and focused on sea breeze effects. We found for a period with low winds, sunny conditions and enhanced $BSOA$ build-up, the sea breeze front passes over the Salles-Bilos measurement site and advects cleaner marine air masses. This manifests as a steep decline of temperature and $BSOA$ at the Salles-Bilos measurements site during afternoon. Thus, advection is important to be considered in addition to

chemistry for well understanding observed time series, even for a measurement site carefully chosen in an environment with a rather homogeneous landcover.

What we have tried to point out here is the necessity of a coupled canopy model or a sub-grid simulation scheme when it comes to simulating areas with particular physical representation like a forest. These types of sub-grid information exist for urban areas or for deserts, but our results show that it is also important to put them into place for forested areas in CTMs. The next steps for this study are to investigate the reasons for the overestimation of the minima concentrations of O_3 inside the forest, as well as the overestimation of the $BSOA$ (for some peaks) after modifications. It is also important to understand the (still) overestimated concentrations of isoprene in the simulations, even after modifications in the tree types and landcover of the area. Further studies should also include the usage of different SOA simulation schemes in order to test their sensitivity to precursor/oxidant changes and the simulated concentrations of $BSOA$. It would be interesting to test the physical parametrization used in this study on other forests to see how the parametrization would perform elsewhere. Another interesting continuation of this work would be making hypothesis about the future of the forest: what effects would climate change modifying the landcover and potentially causing longer periods of drought have on a pine forest and its atmospheric chemistry? This question has become of an even greater importance and sad actuality given the massive forest destructions by the july 2022 fires.

Code and data availability. The model is available for download on the CHIMERE website (CHIMERE, 2023). The WRF model is downloadable on their website (WRF, 2023). ECMWF data are available for download for registered members through request. The measurements can be provided by coauthors upon request. Simulation outputs will be available upon request. All the rest of the inputs/data used in the article are all downloadable free of charge on their respective websites references in the text.

Author contributions. AC has performed the simulations and analyzed them. GS has provided meteorological and general inputs for the simulations. Main preparation of the article has been done by AC and MB. EV, EP, PF, MC, EO have provided measurements used in the article. EV is the responsible of the LABEX/COTE project, which the article is part of. All authors have contributed in rereading and editting the article.

Competing interests. The authors declare that they have no conflict of interest.

Acknowledgements. The authors would like to acknowledge the University of Bordeaux, the CNRS INSU LEFE program and the ANR in the frame of the Investments for the future Program, within the Cluster of Excellence COTE (ANR-10-LABEX-45) for their financial support. This work was granted access to the HPC resources of IDRIS under the allocation 2019-gen7232 and 2021-gen10274 made by GENCI. ATMO-NA (Atmo-Nouvelle-Aquitaine, 2023) is also acknowledged for both the air quality station measurements and the local

anthropogenic emission dataset (Inventaire Atmo Nouvelle-Aquitaine 2014 – ICARE v3.2.1_rev1). They would also like to acknowledge the
805 E-OBS dataset and the data providers in the ECA&D project (Cornes et al., 2018). Copernicus land data is acknowledged for the European forest dataset and also for leaf area index datasets which were generated using Copernicus Atmosphere Monitoring Service Information 2018. Neither the European Commission nor ECMWF is responsible for any use that may be made of the information it contains. IGN (IGN, 2023a) is acknowledged for BDTopo and BDForet datasets.

References

EMEP/EEA air pollutant emission inventory guidebook 2019, https://www.eea.europa.eu/publications/emep-eea-guidebook-2019, https://doi.org/10.2800/293657, accessed: 2022-07-31.

Amedro, D., Miyazaki, K., Parker, A., Schoemaecker, C., and Fittschen, C.: Atmospheric and kinetic studies of OH and HO2 by the FAGE technique, Journal of Environmental Sciences, 24, 78–86, https://doi.org/S1001-0742(11)60723-7, 2012.

Arino, O., Bicheron, P., Achard, F., Latham, J., Witt, R., and Weber, J.-L.: The most detailed portrait of Earth, Eur. Space Agency, 136, 25–31, 2008.

Atmo-Nouvelle-Aquitaine: Atmo-Nouvelle-Aquitaine, https://www.atmo-nouvelleaquitaine.org/, [Online; accessed 18-January-2023], 2023.

Berbigier, P. and Bonnefond, J.: Measurement and modelling of radiation transmission within a stand of maritime pine (Pinus pinaster Ait), in: Annales des sciences forestières, vol. 52, pp. 23–42, EDP Sciences, https://doi.org/10.1051/forest:19950103, 1995.

Bessagnet, B., Menut, L., Curci, G., Hodzic, A., Guillaume, B., Liousse, C., Moukhtar, S., Pun, B., Seigneur, C., and Schulz, M.: Regional modeling of carbonaceous aerosols over Europe—focus on secondary organic aerosols, Journal of Atmospheric Chemistry, 61, 175–202, https://doi.org/10.1007/s10874-009-9129-2, 2008.

Bsaibes, S., Al Ajami, M., Mermet, K., Truong, F., Batut, S., Hecquet, C., Dusanter, S., Léornadis, T., Sauvage, S., Kammer, J., et al.: Variability of hydroxyl radical (OH) reactivity in the Landes maritime pine forest: results from the LANDEX campaign 2017, Atmospheric Chemistry and Physics, 20, 1277–1300, https://doi.org/10.5194/acp-20-1277-2020, 2020.

Carter, W.: SAPRC Atmospheric Chemical Mechanisms and VOC Reactivity Scales, https://intra.engr.ucr.edu/~carter/SAPRC/, [Online; accessed 29-January-2023], 2019.

Carter, W. P.: Development of the SAPRC-07 chemical mechanism, Atmospheric Environment, 44, 5324–5335, https://doi.org/10.1016/j.atmosenv.2010.01.026, 2010.

CHIMERE: CHIMERE chemistry transport model, https://www.lmd.polytechnique.fr/chimere/chimere2020.php, [Online; accessed 18-January-2023], 2023.

Chin, M., Ginoux, P., Kinne, S., Torres, O., Holben, B. N., Duncan, B. N., Martin, R. V., Logan, J. A., Higurashi, A., and Nakajima, T.: Tropospheric aerosol optical thickness from the GOCART model and comparisons with satellite and Sun photometer measurements, Journal of the atmospheric sciences, 59, 461–483, https://doi.org/10.1175/1520-0469(2002)059<0461:TAOTFT>2.0.CO;2, 2002.

Cholakian, A., Beekmann, M., Colette, A., Coll, I., Siour, G., Sciare, J., Marchand, N., Couvidat, F., Pey, J., Gros, V., et al.: Simulation of fine organic aerosols in the western Mediterranean area during the ChArMEx 2013 summer campaign, Atmospheric chemistry and physics, 18, 7287–7312, https://doi.org/10.5194/acp-18-7287-2018, 2018.

Cholakian, A., Beekmann, M., Coll, I., Ciarelli, G., and Colette, A.: Sensitivity of organic aerosol simulation scheme on biogenic organic aerosol concentrations in climate projections, Atmos. Chem. Phys, pp. 13 209–13 226, https://doi.org/10.5194/acp-19-13209-2019, 2019a.

Cholakian, A., Colette, A., Coll, I., Ciarelli, G., and Beekmann, M.: Future climatic drivers and their effect on PM 10 components in Europe and the Mediterranean Sea, Atmospheric Chemistry and Physics, 19, 4459–4484, https://doi.org/10.5194/acp-19-4459-2019, 2019b.

Ciarelli, G., Theobald, M. R., Vivanco, M. G., Beekmann, M., Aas, W., Andersson, C., Bergström, R., Manders-Groot, A., Couvidat, F., Mircea, M., et al.: Trends of inorganic and organic aerosols and precursor gases in Europe: insights from the EURODELTA multi-model experiment over the 1990–2010 period, Geoscientific Model Development, 12, 4923–4954, https://doi.org/10.5194/gmd-12-4923-2019, 2019.

Copernicus: Copernicus land monitoring service, https://land.copernicus.eu/pan-european/high-resolution-layers/forests/, [Online; accessed 18-January-2023], 2023.

Copernicus Land services: Copernicus global land service leaf area index, https://land.copernicus.eu/global/products/lai, [Online; accessed 29-January-2023], 2023.

Cornes, R. C., van der Schrier, G., van den Besselaar, E. J., and Jones, P. D.: An ensemble version of the E-OBS temperature and precipitation data sets, Journal of Geophysical Research: Atmospheres, 123, 9391–9409, https://doi.org/10.1029/2017JD028200, 2018.

DeCarlo, P. F., Kimmel, J. R., Trimborn, A., Northway, M. J., Jayne, J. T., Aiken, A. C., Gonin, M., Fuhrer, K., Horvath, T., Docherty, K. S., et al.: Field-deployable, high-resolution, time-of-flight aerosol mass spectrometer, Analytical chemistry, 78, 8281–8289, https://doi.org/10.1021/ac061249n, 2006.

Delmas, R., Mégie, G., and Peuch, V.: Physique et Chimie de l'Atmosphère, edited by: Belin, 2005.

EMEP: Emissions as used in EMEP models, https://www.ceip.at/webdab-emission-database/emissions-as-used-in-emep-models, [Online; accessed 18-January-2023], 2023.

for Environmental Prediction/National Weather Service/NOAA/US Department of Commerce, N. C.: NCEP FNL operational model global tropospheric analyses, continuing from July 1999, Research Data Archive at the National Center for Atmospheric Research, Computational and Information Systems Laboratory, https://doi.org/10.5065/D6M043C6, 2000.

Fouqueau, A., Cirtog, M., Cazaunau, M., Pangui, E., Zapf, P., Siour, G., Landsheere, X., Méjean, G., Romanini, D., and Picquet-Varrault, B.: Implementation of an incoherent broadband cavity-enhanced absorption spectroscopy technique in an atmospheric simulation chamber for in situ NO3 monitoring: characterization and validation for kinetic studies, Atmospheric Measurement Techniques, 13, 6311–6323, https://doi.org/10.5194/amt-13-6311-2020, 2020.

Giri, C., Zhu, Z., and Reed, B.: A comparative analysis of the Global Land Cover 2000 and MODIS land cover data sets, Remote sensing of environment, 94, 123–132, https://doi.org/10.1016/j.rse.2004.09.005, 2005.

Gray Bé, A., Upshur, M. A., Liu, P., Martin, S. T., Geiger, F. M., and Thomson, R. J.: Cloud activation potentials for atmospheric α-pinene and β-caryophyllene ozonolysis products, ACS central science, 3, 715–725, https://doi.org/10.1021/acscentsci.7b00112, 2017.

Griffin, R. J., Cocker III, D. R., Flagan, R. C., and Seinfeld, J. H.: Organic aerosol formation from the oxidation of biogenic hydrocarbons, Journal of Geophysical Research: Atmospheres, 104, 3555–3567, https://doi.org/10.1029/1998JD100049, 1999.

Guenther, A., Jiang, X., Heald, C. L., Sakulyanontvittaya, T., Duhl, T. a., Emmons, L., and Wang, X.: The Model of Emissions of Gases and Aerosols from Nature version 2.1 (MEGAN2. 1): an extended and updated framework for modeling biogenic emissions, Geoscientific Model Development, 5, 1471–1492, https://doi.org/10.5194/gmd-5-1471-2012, 2012.

Guenther, A., Jiang, X., Shah, T., Huang, L., Kemball-Cook, S., and Yarwood, G.: Model of emissions of gases and aerosol from nature version 3 (MEGAN3) for estimating biogenic emissions, in: International Technical Meeting on Air Pollution Modelling and its Application, pp. 187–192, Springer, https://doi.org/10.1007/978-3-030-22055-6_29, 2018.

Gutman, G., Byrnes, R. A., Masek, J., Covington, S., Justice, C., Franks, S., and Headley, R.: Towards monitoring land-cover and land-use changes at a global scale: The Global Land Survey 2005, Photogrammetric Engineering and Remote Sensing, 74, 6–10, 2008.

Hallquist, M., Wenger, J. C., Baltensperger, U., Rudich, Y., Simpson, D., Claeys, M., Dommen, J., Donahue, N., George, C., Goldstein, A., et al.: The formation, properties and impact of secondary organic aerosol: current and emerging issues, Atmospheric chemistry and physics, 9, 5155–5236, https://doi.org/10.5194/acp-9-5155-2009, 2009.

Hantson, S., Knorr, W., Schurgers, G., Pugh, T. A., and Arneth, A.: Global isoprene and monoterpene emissions under changing climate, vegetation, CO2 and land use, Atmospheric Environment, 155, 35–45, https://doi.org/10.1016/j.atmosenv.2017.02.010, 2017.

Hassika, P., Berbigier, P., and Bonnefond, J.: Measurement and modelling of the photosynthetically active radiation transmitted in a canopy of maritime pine, in: Annales des sciences forestières, vol. 54, pp. 715–730, EDP Sciences, https://doi.org/10.1051/forest:19970803, 1997.

Hauglustaine, D. A., Balkanski, Y., and Schulz, M.: A global model simulation of present and future nitrate aerosols and their direct radiative forcing of climate, Atmospheric Chemistry and Physics, 14, 11 031–11 063, https://doi.org/10.5194/acp-14-11031-2014, 2014.

Hellén, H., Praplan, A. P., Tykkä, T., Ylivinkka, I., Vakkari, V., Bäck, J., Petäjä, T., Kulmala, M., and Hakola, H.: Long-term measurements of volatile organic compounds highlight the importance of sesquiterpenes for the atmospheric chemistry of a boreal forest, Atmospheric Chemistry and Physics, 18, 13 839–13 863, https://doi.org/10.5194/acp-18-13839-2018, 2018.

Hughes, C. P. and Veron, D. E.: A characterization of the Delaware sea breeze using observations and modeling, Journal of Applied Meteorology and Climatology, 57, 1405–1421, https://doi.org/10.1175/JAMC-D-17-0186.1, 2018.

ICOS: ICOS Salles station description, https://xylofront.pierroton.inra.fr/Salles2.html, [Online; accessed 18-January-2023], 2023.

IGN: Institut national de l'information géographiques et forestière, https://www.ign.fr/, [Online; accessed 18-January-2023], 2023a.

IGN: Institut national de l'information géographiques et forestière, https://www.theia-land.fr/en/homepage-en/, [Online; accessed 18-January-2023], 2023b.

Kammer, J., Perraudin, E., Flaud, P.-M., Lamaud, E., Bonnefond, J.-M., and Villenave, E.: Observation of nighttime new particle formation over the French Landes forest, Science of The Total Environment, 621, 1084–1092, https://doi.org/10.1016/j.scitotenv.2017.10.118, 2018.

Kammer, J., Flaud, P.-M., Chazeaubeny, A., Ciuraru, R., Le Menach, K., Geneste, E., Budzinski, H., Bonnefond, J., Lamaud, E., Perraudin, E., et al.: Biogenic volatile organic compounds (BVOCs) reactivity related to new particle formation (NPF) over the Landes forest, Atmospheric Research, 237, 104 869, https://doi.org/10.1016/j.atmosres.2020.104869, 2020.

Kulmala, M., Suni, T., Lehtinen, K., Dal Maso, M., Boy, M., Reissell, A., Rannik, Ü., Aalto, P., Keronen, P., Hakola, H., et al.: A new feedback mechanism linking forests, aerosols, and climate, Atmospheric Chemistry and Physics, 4, 557–562, https://doi.org/10.5194/acp-4-557-2004, 2004.

LabEx: LabEx COTE, https://cote.labex.u-bordeaux.fr/, [Online; accessed 18-January-2023], 2023.

Lachatre, M., Fortems-Cheiney, A., Foret, G., Siour, G., Dufour, G., Clarisse, L., Clerbaux, C., Coheur, P.-F., Van Damme, M., and Beekmann, M.: The unintended consequence of SO2 and NO2 regulations over China: increase of ammonia levels and impact on PM2.5 concentrations, Atmospheric Chemistry and Physics, 19, 6701–6716, https://doi.org/10.5194/acp-19-6701-2019, 2019.

Lapere, R., Menut, L., Mailler, S., and Huneeus, N.: Soccer games and record-breaking PM 2.5 pollution events in Santiago, Chile, Atmospheric Chemistry and Physics, 20, 4681–4694, https://doi.org/10.5194/acp-20-4681-2020, 2020.

Lee, A., Goldstein, A. H., Keywood, M. D., Gao, S., Varutbangkul, V., Bahreini, R., Ng, N. L., Flagan, R. C., and Seinfeld, J. H.: Gas-phase products and secondary aerosol yields from the ozonolysis of ten different terpenes, Journal of Geophysical Research: Atmospheres, 111, https://doi.org/10.1029/2005JD006437, 2006a.

Lee, A., Goldstein, A. H., Kroll, J. H., Ng, N. L., Varutbangkul, V., Flagan, R. C., and Seinfeld, J. H.: Gas-phase products and secondary aerosol yields from the photooxidation of 16 different terpenes, Journal of Geophysical Research: Atmospheres, 111, https://doi.org/10.1029/2006JD007050, 2006b.

Lemaire, V., Coll, I., Couvidat, F., Mouchel-Vallon, C., Seigneur, C., and Siour, G.: Oligomer formation in the troposphere: from experimental knowledge to 3-D modeling, Geoscientific Model Development, 9, 1361–1382, https://doi.org/10.5194/gmd-9-1361-2016, 2016.

Lerczak, J. A., Hendershott, M., and Winant, C.: Observations and modeling of coastal internal waves driven by a diurnal sea breeze, Journal of Geophysical Research: Oceans, 106, 19 715–19 729, https://doi.org/10.1029/2010JD015367, 2001.

Leuning, R.: Estimation of scalar source/sink distributions in plant canopies using Lagrangian dispersion analysis: Corrections for atmospheric stability and comparison with a multilayer canopy model, Boundary-Layer Meteorology, 96, 293–314, https://doi.org/10.1023/A:1002449700617, 2000.

Li, H., Riva, M., Rantala, P., Heikkinen, L., Daellenbach, K., Krechmer, J. E., Flaud, P.-M., Worsnop, D., Kulmala, M., Villenave, E., et al.: Terpenes and their oxidation products in the French Landes forest: insights from Vocus PTR-TOF measurements, Atmospheric Chemistry and Physics, 20, 1941–1959, https://doi.org/10.5194/acp-20-1941-2020, 2020.

Li, H., Canagaratna, M. R., Riva, M., Rantala, P., Zhang, Y., Thomas, S., Heikkinen, L., Flaud, P.-M., Villenave, E., Perraudin, E., et al.: Atmospheric organic vapors in two European pine forests measured by a Vocus PTR-TOF: insights into monoterpene and sesquiterpene oxidation processes, Atmospheric Chemistry and Physics, 21, 4123–4147, https://doi.org/10.5194/acp-21-4123-2021, 2021.

Mailler, S., Menut, L., Khvorostyanov, D., Valari, M., Couvidat, F., Siour, G., Turquety, S., Briant, R., Tuccella, P., Bessagnet, B., et al.: CHIMERE-2017: From urban to hemispheric chemistry-transport modeling, Geoscientific Model Development, 10, 2397–2423, https://doi.org/10.5194/gmd-10-2397-2017, 2017.

Menut, L., Bessagnet, B., Khvorostyanov, D., Beekmann, M., Blond, N., Colette, A., Coll, I., Curci, G., Foret, G., Hodzic, A., et al.: CHIMERE 2013: a model for regional atmospheric composition modelling, Geoscientific model development, 6, 981–1028, https://doi.org/10.5194/gmd-6-981-2013, 2013.

Mermet, K., Sauvage, S., Dusanter, S., Salameh, T., Léonardis, T., Flaud, P.-M., Perraudin, É., Villenave, É., and Locoge, N.: Optimization of a gas chromatographic unit for measuring biogenic volatile organic compounds in ambient air, Atmospheric Measurement Techniques, 12, 6153–6171, https://doi.org/10.5194/amt-12-6153-2019, 2019.

Mermet, K., Perraudin, E., Dusanter, S., Sauvage, S., Léonardis, T., Flaud, P.-M., Bsaibes, S., Kammer, J., Michoud, V., Gratien, A., et al.: Atmospheric reactivity of biogenic volatile organic compounds in a maritime pine forest during the LANDEX episode 1 field campaign, Science of the Total Environment, 756, 144 129, https://doi.org/10.1016/j.scitotenv.2020.144129, 2021.

Moreaux, V., Lamaud, É., Bosc, A., Bonnefond, J.-M., Medlyn, B. E., and Loustau, D.: Paired comparison of water, energy and carbon exchanges over two young maritime pine stands (Pinus pinaster Ait.): effects of thinning and weeding in the early stage of tree growth, Tree physiology, 31, 903–921, https://doi.org/10.1093/treephys/tpr048, 2011.

Ng, N., Chhabra, P., Chan, A., Surratt, J., Kroll, J., Kwan, A., McCabe, D., Wennberg, P., Sorooshian, A., Murphy, S., et al.: Effect of NO x level on secondary organic aerosol (SOA) formation from the photooxidation of terpenes, Atmospheric Chemistry and Physics, 7, 5159–5174, https://doi.org/10.5194/acp-7-5159-2007, 2007.

Ng, N. L., Brown, S. S., Archibald, A. T., Atlas, E., Cohen, R. C., Crowley, J. N., Day, D. A., Donahue, N. M., Fry, J. L., Fuchs, H., et al.: Nitrate radicals and biogenic volatile organic compounds: oxidation, mechanisms, and organic aerosol, Atmospheric chemistry and physics, 17, 2103–2162, https://doi.org/10.5194/acp-17-2103-2017, 2017.

Odum, J., Hoffmann, T., Bowman, F., Collins, D., Flagan, R., and Seinfeld, J.: Gas-Particle Partitioning and Secondary Organic Aerosol Yields, https://doi.org/10.1021/ES950943+, 1996.

Ogée, J., Brunet, Y., Loustau, D., Berbigier, P., and Delzon, S.: MuSICA, a CO2, water and energy multilayer, multileaf pine forest model: evaluation from hourly to yearly time scales and sensitivity analysis, Global Change Biology, 9, 697–717, https://doi.org/10.1046/j.1365-2486.2003.00628.x, 2003.

Owens, R. and Hewson, T.: ECMWF forecast user guide, Reading: ECMWF, 10, m1cs7h, https://doi.org/10.21957/m1cs7h, 2018.

Pankow, J. F.: Review and comparative analysis of the theories on partitioning between the gas and aerosol particulate phases in the atmosphere, Atmospheric Environment (1967), 21, 2275–2283, https://doi.org/10.1016/0004-6981(87)90363-5, 1987.

Planchon, O. and Cautenet, S.: Rainfall and sea-breeze circulation over south-western France, International Journal of Climatology: A Journal of the Royal Meteorological Society, 17, 535–549, https://doi.org/10.1002/(SICI)1097-0088(199704)17:5<535::AID-JOC150>3.0.CO;2-L, 1997.

Pun, B. and Seigneur, C.: Investigative modeling of new pathways for secondary organic aerosol formation, Atmospheric Chemistry and Physics, 7, 2199–2216, https://doi.org/10.5194/acp-7-2199-2007, 2007.

Qin, M., Hu, Y., Wang, X., Vasilakos, P., Boyd, C. M., Xu, L., Song, Y., Ng, N. L., Nenes, A., and Russell, A. G.: Modeling biogenic secondary organic aerosol (BSOA) formation from monoterpene reactions with NO3: A case study of the SOAS campaign using CMAQ, Atmospheric Environment, 184, 146–155, https://doi.org/10.1016/j.atmosenv.2018.03.042, 2018.

Sartelet, K. N., Couvidat, F., Seigneur, C., and Roustan, Y.: Impact of biogenic emissions on air quality over Europe and North America, Atmospheric Environment, 53, 131–141, https://doi.org/10.1016/j.atmosenv.2011.10.046, 2012.

Seinfeld, J. and Pandis, S.: Atmospheric chemistry and physics: from air pollution to climate change, vol. 40, Taylor & Francis, 2016.

Shrivastava, M., Andreae, M. O., Artaxo, P., Barbosa, H. M., Berg, L. K., Brito, J., Ching, J., Easter, R. C., Fan, J., Fast, J. D., et al.: Urban pollution greatly enhances formation of natural aerosols over the Amazon rainforest, Nature communications, 10, 1–12, https://doi.org/10.1038/s41467-019-08909-4, 2019.

Simon, V., Luchetta, L., and Torres, L.: Estimating the emission of volatile organic compounds (VOC) from the French forest ecosystem, Atmospheric Environment, 35, S115–S126, https://doi.org/10.1016/S1352-2310(00)00565-3, 2001.

Sporre, M. K., Blichner, S. M., Karset, I. H., Makkonen, R., and Berntsen, T. K.: BVOC–aerosol–climate feedbacks investigated using NorESM, Atmospheric Chemistry and Physics, 19, 4763–4782, https://doi.org/10.5194/acp-19-4763-2019, 2019.

Trewhela, B., Huneeus, N., Munizaga, M., Mazzeo, A., Menut, L., Mailler, S., Valari, M., and Ordoñez, C.: Analysis of exposure to fine particulate matter using passive data from public transport, Atmospheric Environment, 215, 116 878, https://doi.org/10.1016/j.atmosenv.2019.116878, 2019.

Troen, I. and Mahrt, L.: A simple model of the atmospheric boundary layer; sensitivity to surface evaporation, Boundary-Layer Meteorology, 37, 129–148, https://doi.org/10.1007/BF00122760, 1986.

Wang, W., Bruyère, C., Duda, M., Dudhia, J., Gill, D., Kavulich, M., Keene, K., Lin, H., Michalakes, J., Rizvi, S., et al.: WRF ARW Version 3 Modeling System User's Guide, 1–428, https://doi.org/10.1525/jps.2007.37.1.204, 2015.

WRF: Weather Research and Forecast, https://github.com/wrf-model/WRF, [Online; accessed 18-January-2023], 2023.

Xu, L., Guo, H., Boyd, C. M., Klein, M., Bougiatioti, A., Cerully, K. M., Hite, J. R., Isaacman-VanWertz, G., Kreisberg, N. M., Knote, C., et al.: Effects of anthropogenic emissions on aerosol formation from isoprene and monoterpenes in the southeastern United States, Proceedings of the National Academy of Sciences, 112, 37–42, https://doi.org/10.1073/pnas.1417609112, 2015.